



Defence Research and
Development Canada

Recherche et développement
pour la défense Canada



Evaluation of Simulated RADARSAT-2 Polarimetry Products

Chen Liu and Paris W. Vachon

Defence R&D Canada – Ottawa
TECHNICAL MEMORANDUM
DRDC Ottawa TM 2007-189
September 2007

Canada

Evaluation of Simulated RADARSAT-2 Polarimetry Products

Chen Liu and Paris W. Vachon
DRDC Ottawa

Defence R&D Canada – Ottawa

Technical Memorandum
DRDC Ottawa TM 2007-189
September 2007

Principal Author

Original signed by Chen Liu

Chen Liu

Defence Scientist

Approved by

Original signed by David Schlingmeier

David Schlingmeier

A/Head, Radar Applications and Space Technologies Section

Approved for release by

Original signed by Pierre Lavoie

Pierre Lavoie

Chair, Document Review Panel

- © Her Majesty the Queen as represented by the Minister of National Defence, 2007.
- © Sa Majesté la Reine, représentée par le ministre de la Défense nationale, 2007.

Abstract

This report presents an evaluation of simulated RADARSAT-2 polarimetry products. The RSAT2SIMU software developed by MDA was used to simulate RADARSAT-2 products from Environment Canada (EC) CV-580 synthetic aperture radar (SAR) single-look complex (SLC) data by increasing the noise floor and degrading the image resolution. The evaluation includes assessment of the reduction in the probability of missed detection for polarimetric relative to single channel radar operation for ship detection, and the potential benefit of polarimetric target decomposition to generate ship target classification features and to segment the ship target of interest from the ocean background. A key recommendation is to develop algorithms that combine all information available from polarimetric signature analysis methods to aid in ship classification. The results show that the ship detection and target classification methods developed using airborne polarimetric SAR data can potentially be applied to RADARSAT-2 data.

Résumé

Le présent rapport évalue des produits de polarimétrie RADARSAT-2 simulés. Le logiciel RSAT2SIMU créé par MDA a servi à simuler des produits de RADARSAT-2 tirés de données singulières complexes (SLC) du radar à synthèse d'ouverture (RSO) CV-580 d'Environnement Canada (EC) par l'élévation du seuil de bruit et la dégradation de la résolution d'image.

L'évaluation vise à déterminer la réduction de la probabilité de détection manquée de la polarimétrie comparativement à l'utilisation d'un radar monocanal pour détecter des navires ainsi que les avantages possibles de la décomposition des cibles polarimétriques pour générer les caractéristiques de classification des cibles de navire et pour segmenter une cible de navire d'intérêt par rapport au fond océanique. Une recommandation clé consiste à établir des algorithmes combinant toute l'information obtenue selon des méthodes d'analyse des signatures polarimétriques afin de faciliter la classification des navires. Les résultats révèlent que les méthodes de détection des navires et de classification des cibles, qui se fondent sur des données polarimétriques de RSO aéroporté, pourraient éventuellement être appliquées aux données de RADARSAT-2.

Executive summary

Evaluation of Simulated RADARSAT-2 Polarimetry Products

Liu, Chen; Vachon, Paris W.; DRDC Ottawa TM 2007-189; Defence R&D Canada – Ottawa; September 2007.

Introduction

RADARSAT-2, which is expected to be launched in late 2007, will carry a C-band synthetic aperture radar (SAR) that will offer many operational modes such as polarimetric SAR (PolSAR). A PolSAR system alternately transmits horizontally (H) and vertically (V) polarized electromagnetic pulses, and then measures both the horizontally (H) and vertically (V) polarized scattered fields. There are four possible combinations of incident and scattered electric fields, HH, HV, VH, and VV. RADARSAT-2 will offer quadrature polarization (quad-pol), selective polarization (HH and HV or VH and VV), and selective single polarization (HH or HV or VH or VV).

Previous studies have shown that there is a significant improvement in ship detection sensitivity and a reduction in false alarm rate by using PolSAR data, especially for small ships. The greatest improvement is obtained with quad polarimetric data. However, the swath width which can be covered is reduced due to system bandwidth constraints. Good performance can also be obtained with dual co-polarization with phase, which in principle provides a wider swath width due to reduced bandwidth requirements. Performance is characterized by the probability of missed detection as a function of false alarm probability.

The present study investigates the feasibility of applying algorithms for improving ship detection and classification by using airborne PolSAR data converted to simulated RADARSAT-2 polarimetry products. The PolSAR ship detection algorithm used in this study was developed at DRDC Ottawa. Three target classification methods were applied: Pauli, Cameron, and the symmetric scattering characterization method (SSCM). The software for the Pauli and the Cameron methods were developed at DRDC Ottawa, while the SSCM tool was implemented in a PolSAR workstation that was developed at the Canada Centre for Remote Sensing (CCRS) and was made available to DRDC Ottawa by the Canadian Space Agency (CSA).

The RADARSAT-2 images were simulated using the RADARSAT-2 simulator (RSAT2SIMU) that was developed by MDA and was also made available to DRDC Ottawa by CSA. The RSAT2SIMU software simulates RADARSAT-2 products from Environment Canada (EC) CV-580 C-band polarimetric SAR products in single-look complex (SLC) format by appropriately increasing the noise floor and degrading the spatial resolution. However, the simulator can not account for the specific geometry of RADARSAT-2, that is, the altitude, incidence angle, and swath coverage. The simulated data quality depends on the input CV-580 SAR data quality.

The input CV-580 data considered in this work was obtained during the Maritime Sensor Integration Experiment (MARSIE) trial. The data set includes several known ships including the 25 m long *Dominion Victory*.

Significance

This study demonstrates that the algorithms developed for improving ship detection and classification using airborne PolSAR data will also be applicable to RADARSAT-2 polarimetric data. The results demonstrate the significant improvement in ship detection performance that is expected from using polarimetric data. Furthermore, it is shown that the polarimetric signature of a target may also improve ship classification performance.

Results

For ship detection, the results show the advantage of polarimetric systems. For example, the dual co-polarization system with phase provides better detection performance than single channel HH polarization. In principle, a dual co-polarization system could provide a wider swath coverage than a polarimetric system.

For target classification, the Cameron and SSCM target decomposition methods provide unique information on the distribution and types of scatterers that constitute the target of interest, providing an approach for target classification. These decomposition methods work best for well-focused, large ships. The Pauli decomposition method provides a simple but efficient way to segment the target of interest from the surrounding ocean clutter.

Future Plans

The results demonstrate that target decomposition and polarimetric signature analysis may improve target classification. To achieve target classification, the following issues are recommended for further study:

- The relationship between the physical properties of the target and the elemental scatterers derived from the Cameron and the SSCM polarimetric decomposition methods;
- The feasibility of applying polarimetric decomposition methods to automatic target recognition (ATR) algorithms by using scattering elements or estimated scatterer orientation angles as target features in target classification software; and
- The development of algorithms that fuse all information available from polarimetric signature analysis methods to aid in ship classification.

Sommaire

Evaluation of Simulated RADARSAT-2 Polarimetry Products

Liu, Chen; Vachon, Paris W.; DRDC Ottawa TM 2007-189; R & D pour la défense Canada – Ottawa; September 2007.

Introduction

RADARSAT-2, qui devrait être lancé vers la fin de 2007, transportera un radar à synthèse d'ouverture (RSO) à bande C qui offrira de nombreux modes de fonctionnement, comme celui du RSO polarimétrique (PolSAR). Un système PolSAR émet alternativement des impulsions électromagnétiques à polarisations horizontale (H) et verticale (V), puis mesure les champs diffusés à polarisations horizontale (H) et verticale (V). Il existe quatre combinaisons possibles de champs électriques incidents et diffusés, HH, HV, VH et VV. RADARSAT-2 offrira la quadrature polarisation (quad-pol), la polarisation sélective (HH et HV ou VH et VV), ainsi que la polarisation simple sélective (HH ou HV ou VH ou VV).

Des études antérieures ont démontré que l'utilisation des données de PolSAR peut améliorer considérablement la sensibilité de détection des navires et réduire le taux de fausses alertes, surtout pour les petits navires. Les données à quadruple polarisation procurent la plus grande amélioration. La largeur de balayage couverte est toutefois réduite en raison des contraintes de largeur de bande du système. La double copolarisation avec phase, qui augmente en principe la largeur de balayage par la réduction de la largeur de bande requise, permet aussi d'obtenir un bon rendement. Le rendement se caractérise par la probabilité de détection manquée en fonction de la probabilité de fausse alarme.

La présente étude examine la possibilité d'appliquer des algorithmes pour améliorer la détection et la classification des navires par l'utilisation de données d'un PolSAR aéroporté converties en produits de polarimétrie simulés de RADARSAT-2. L'algorithme de détection des navires de PolSAR, qui a été utilisé pour cette étude, a été mis au point à RDDC Ottawa. Trois méthodes de classification des cibles ont été appliquées : les méthodes de Pauli, de Cameron et de caractérisation de diffusion symétrique (SSCM). Le logiciel utilisé pour les méthodes de Pauli et de Cameron a été mis au point à RDDC Ottawa, tandis que l'outil SSCM a été incorporé à un poste de travail PolSAR développé au Centre canadien de télédétection (CCT) et mis à la disposition de RDDC Ottawa par l'Agence spatiale canadienne (ASC).

Les images de RADARSAT-2 ont été simulées à l'aide du simulateur RADARSAT-2 (RSAT2SIMU) mis au point par MDA et ont également été mises à la disposition de RDDC Ottawa par l'ASC. Le logiciel RSAT2SIMU simule les produits RADARSAT-2 provenant du RSO polarimétrique à bande C CV-580 d'Environnement Canada (EC), dans un format singulier complexe (SLC), en élévant correctement le seuil de bruit et en dégradant la résolution spatiale. Le simulateur ne peut toutefois pas tenir compte de la géométrie particulière de RADARSAT-2, c'est-à-dire de l'altitude, de l'angle d'incidence et de la couverture du balayage. La qualité des données simulées dépend de la qualité des données de RSO CV-580 fournies à l'entrée.

Les données d'entrée de CV-580 utilisées pour ces travaux ont été tirées de l'expérience sur l'intégration des capteurs maritimes (MARSIE). L'ensemble de données a trait à plusieurs navires connus, notamment le *Dominion Victory* d'une longueur de 25 m.

Portée

L'étude démontre que les algorithmes mis au point pour améliorer la détection et la classification des navires à l'aide des données de PolSAR aéroporté s'appliqueront aussi aux données polarimétriques de RADARSAT-2. Les résultats mettent en évidence l'amélioration significative du rendement de détection des navires, que devrait procurer l'utilisation de données polarimétriques. De plus, il est démontré que la signature polarimétrique d'une cible peut améliorer le rendement de classification des navires.

Résultats

Pour la détection des navires, les résultats font ressortir l'avantage des systèmes polarimétriques. Par exemple, la double copolarisation avec phase offre un meilleur rendement de détection que la polarisation HH monocanal. En principe, un système à double copolarisation pourrait produire une plus large couverture de balayage qu'un système polarimétrique.

Pour la classification des cibles, les méthodes de décomposition des cibles de Cameron et SSCM fournissent de l'information unique sur la répartition et les types de diffuseurs qui constituent les cibles d'intérêt, offrant ainsi une technique de classification des cibles. Ces méthodes de décomposition s'avèrent particulièrement efficaces pour les gros navires bien ciblés. La méthode de décomposition de Pauli offre un moyen simple mais efficace de segmenter la cible d'intérêt par rapport au clutter océanique environnant.

Recherches futures

Les résultats démontrent que la décomposition des cibles et l'analyse des signatures polarimétriques peuvent améliorer la classification des cibles. Pour la classification des cibles, les aspects suivants sont recommandés en vue de recherches futures :

- Relations entre les propriétés physiques des cibles et des diffuseurs élémentaires, selon les méthodes de décomposition polarimétrique de Cameron et SSCM.
- Possibilité d'application des méthodes de décomposition polarimétrique aux algorithmes de reconnaissance automatique des cibles (ATR) par l'utilisation des éléments de diffusion ou des angles estimés d'orientation des diffuseurs comme caractéristiques des cibles dans le logiciel de classification des cibles.
- Établissement d'algorithmes fusionnant toute l'information obtenue des méthodes d'analyse des signatures polarimétriques pour faciliter la classification des navires.

Table of contents

Abstract	i
Résumé	ii
Executive summary	iii
Sommaire.....	v
Table of contents	vii
List of figures	ix
List of tables	xii
Acknowledgements	xiii
1. Introduction.....	1
1.1 Polarimetric data from the MARSIE trial.....	1
1.2 Methodology	2
1.3 Outline of this document	2
2. RADARSAT-2 Capabilities	3
3. RADARSAT-2 simulator	4
3.1 Simulation process.....	4
3.2 Differences with respect to RADARSAT-2 products	5
4. Overview of analysis methods	7
4.1 Receiver operating characteristic.....	7
4.2 Polarimetric target decomposition.....	9
4.2.1 Pauli	9
4.2.2 Cameron	9
4.2.3 Symmetric Scattering Characterization Method	11
5 Polarimetric SAR data	13
5.1 Data description.....	13
5.2 Data quality evaluation.....	13
6 Analysis results	20
6.1 Simulated vessel images.....	20
6.2 Receiver Operating Characteristic	21
6.3 Target decomposition	22
6.3.1 Pauli	23
6.3.2 Cameron	24
6.3.3 SSCM	25
7 Summary and conclusions	31
Annex A Simulated RADARSAT-2 images	35
Annex B ROC	41

Annex C Pauli Decomposition Results	43
Annex D Camerom decomposition results.....	45
Annex E SSCM decomposition results	49
Annex F Ship photos	53
List of symbols/abbreviations/acronyms/initialisms	54

List of figures

Figure 1: RADARSAT-2 operation modes and coverage (used with permission [1]).	3
Figure 2: CV-580 data input to RSAT2SIMU.....	5
Figure 3: Simulated RADARSAT-2 images; a) Fine Quad-Pol Mode: b) Standard Quad-Pol Mode.	5
Figure 4: Physical interpretation of three basic scattering mechanisms.....	9
Figure 5: Unit disk representation of symmetric scatterers.	10
Figure 6: Poincaré sphere representation of symmetric scatterers (use with permission [7]).	11
Figure 7: Corner reflectors and calibration site in HH images (11p8, 24 September 2002); a) CV-580; b) simulated RADARSAT-2 Fine Quad-Pol Mode; c) simulated RADARSAT-2 Standard Quad-Pol Mode.	15
Figure 8: Calibration site and 75 cm corner reflector in a RADARSAT-1 image (7 May 2004).	16
Figure 9: Simulated RADARSAT-2 images of urban environment (11p8, 24 September 2002); a) Fine Quad-Pol Mode; b) Standard Quad-Pol Mode.	18
Figure 10: RADARSAT-1 image of urban environment (7 May 2004).	19
Figure 11: Polarimetric image of Dominion Victory (l41p1, 20 October 2005); a) CV-580; b) simulated RADARSAT-2 Fine Quad-Pol Mode; c) simulated RADARSAT-2 Standard Quad-Pol Mode.	21
Figure 12: Detection performance for Dominion Victory (l41p1, 20 October 2005). a) Fine Quad-Pol Mode; b) Standard Quad-Pol Mode.	22
Figure 13: Pauli decomposition images of Dominion Victory (l41p1 20 October 2005). a) Fine Quad-Pol Mode; b) Standard Quad-Pol Mode.	23
Figure 14: Cameron decomposition image (left) and histogram (right) of Dominion Victory (l41p1 20 October 2005). Top: Fine Quad-Pol, Bottom: Standard Quad-Pol.....	24
Figure 15: SSCM decomposition images of Dominion Victory (l41p1, 20 October 2005). Top: Fine Quad-Pol Mode; bottom: Standard Quad-Pol Mode. Left: Latitude coordinate; right: Longitude coordinate.....	26
Figure 16: SSCM classification image (left) and histogram (right) of Dominion Victory (l41p1, 20 October 2005). Top: Fine Quad-Pol Mode; bottom: Standard Quad-Pol Mode.	27
Figure 17: SSCM results of HMCS Toronto (l22p2, 17 October 2005) of Fine Quad-Pol Mode. a) latitude; b) longitude; c) classification and d) classification histogram.....	28
Figure 18: SSCM results of HMCS Toronto (l22p2, 17 October 2005) of Standard Quad-Pol Mode. a) latitude; b) longitude; c) classification and d) classification histogram.....	29
Figure 19: Polarimetric image of Dominion Victory (l41p2, 20 October 2005). a) CV-580 image; b) Fine Quad-Pol Mode; c) Standard Quad-Pol Mode.	35

Figure 20: Polarimetric image of Dominion Victory (l41p3, 20 October 2005). a) CV-580 image; b) Fine Quad-Pol Mode; c) Standard Quad-Pol Mode.....	36
Figure 21: Polarimetric image of Dominion Victory (l42p4, 20 October 2005). a) CV-580 image; b) Fine Quad-Pol Mode; c) Standard Quad-Pol Mode.....	37
Figure 22: Polarimetric image of Gulf Service (l22p2, 17 October 2005). a) CV-580 image; b) Fine Quad-Pol Mode; c) Standard Quad-Pol Mode.	38
Figure 23: Polarimetric image of Edward Cornwallis (l22p2, 17 October 2005). a) CV-580 image; b) Fine Quad-Pol Mode; c) Standard Quad-Pol Mode.	39
Figure 24: Polarimetric image of HMCS Toronto (l22p2, 17 October 2005). a) CV-580 image; b) Fine Quad-Pol Mode; c) Standard Quad-Pol Mode.	40
Figure 25: Detection performance for Dominion Victory (l41p2, 20 October 2005). a) Fine Quad-Pol Mode; b). Standard Quad-Pol Mode.	41
Figure 26: Detection performance for Dominion Victory (l41p3, 20 October 2005). a). Fine Quad-Pol Mode; b). Standard Quad-Pol Mode.	41
Figure 27: Detection performance for Dominion Victory (l42p4, 20 October 2005). a) Fine Quad-Pol Mode; b) Standard Quad-Pol Mode.	42
Figure 28: Pauli decomposition image of Dominion Victory (l41p3, 20 October 2005). a) Fine Quad-Pol Mode; b) Standard Quad-Pol Mode.	43
Figure 29: Pauli decomposition image of Dominion Victory (l42p2, 20 October 2005). a) Fine Quad-Pol Mode; b) Standard Quad-Pol Mode.	43
Figure 30: Pauli decomposition image of Gulf Service (l42p2, 17 October 2005). a) Fine Quad-Pol Mode; b) Standard Quad-Pol Mode.	44
Figure 31: Pauli decomposition image of HMCS Toronto (l22p2, 17 October 2005). a) Fine Quad-Pol Mode; b) standard quad-plo Mode.	44
Figure 32: Cameron decomposition image and histogram of Dominion Victory(l41p3, 20 October 2005). a) Fine Quad-Pol Mode; b) Standard Quad-Pol Mode.....	45
Figure 33: Cameron decomposition image and histogram of Dominion Victory (l42p4, 20 October 2005). a) Fine Quad-Pol Mode; b) Standard Quad-Pol Mode.....	46
Figure 34: Cameron decomposition image and histogram of Gulf Servic (l22p2, 17 October 2005). a) Fine Quad-Pol Mode; b) standard quad-plo Mode.	47
Figure 35: Cameron decomposition image and histogram of HMCS Toronto (l22p2, 17 October 2005). a) Fine Quad-Pol Mode; b)standard quad-plo Mode.	48
Figure 36: SSCM decomposition images Gulf Service for Fine Quad-Pol Mode (l22p2, 17 October 2005). a) latitude; b) longitude; c) classification; d) histogram.	49
Figure 37: SSCM decomposition images of Gulf Service for Standare Quad-Pol Mode (l22p2, 17 October 2005). a) latitude; b) longitude; c) classification; d) histogram. ..	50
Figure 38: SSCM decomposition images of Toronto for Fine Quad-Pol mode (l22p2, 17 October 2005). a) latitude; b) longitude; c) classification; d) histogram.	51

Figure 39: SSCM decomposition images of Toronto for Standard Quad-Pol mode (I22p2, 17 October 2005). a) latitude; b) longitude; c) classification; d) histogram.	52
Figure 40: Ship photographs: a) Dominion Victory; b) HMCS Toronto; c) Gulf Service.	53

List of tables

Table 1: Key parameters of RADARSAT-2 polarimetric image modes.....	3
Table 2: Key system parameters for the CV-580 and RADARSAT-2 SARs.....	4
Table 3. Elemental scatterer coordinates on the Poincaré sphere.....	11
Table 4: threshold to generate each symmetric scatterer.....	12
Table 5: CV-580 data used in the RADARSAT-2 simulations.....	13
Table 6: Ships used in the analysis.....	13
Table 7: Statistical parameters of a corner reflector and the image resolution.....	17
Table 8: Values of P_{MD} for $P_{FA} = 10^{-4}$ for Dominion Victory.....	22
Table 9: Decomposition analysis thresholds.....	23
Table 10: Summary of elemental scatterer distributions for Cameron decomposition for simulated Fine Quad-Pol images.....	25
Table 11: Summary of elemental scatterer distributions for Cameron decomposition for Standard Quad-Pol images	25
Table 12: Summary of element scatterer distributions of SSCM decomposition for Fine Quad-Pol Mode.....	29
Table 13: Summary of element scatterer distributions of SSCM decomposition for Standard Quad-Pol Mode.....	30

Acknowledgements

The authors are grateful for having had the opportunity to use the MARSIE trial PolSAR data, the Polarimetry Workstation (PWS) software, and the RADARSAT-2 Simulator (RSAT2SIMU) software.

The MARSIE trial was implemented as a TTCP SEN AG-7 activity with Gary Geling (DRDC Ottawa) and LCdr Anthony Cond (DRDC) as the Chief Scientist and Experiment Coordinator, respectively. The PolSAR data acquisition was supported by Project Polar Epsilon and DRDC Ottawa.

The PWS software was developed by CCRS and was made available to DRDC Ottawa by the Canadian Space Agency (CSA).

The RSAT2SIMU software was developed by MDA and was also made available to DRDC Ottawa by CSA.

We thank Dr. Ronald Caves (MDA) for helpful discussions concerning use of the RSAT2SIMU software. We thank Terry Potter, Bing Yue, and Vijay Singh (DRDC Ottawa contractors) for their contributions to the PolSAR data processing, RADARSAT-2 data simulation, and data analysis.

This page intentionally left blank.

1. Introduction

Spaceborne C-band polarimetric synthetic aperture radar capabilities will become operationally available in the near future. RADARSAT-2 is expected to be launched in 2007 and will provide many features, including quadrature polarization (quad-pol), selective polarization (HH and HV or VH and VV), and selective single polarization (HH or HV or VH or VV) [1], where the H and V represent horizontal and vertical polarization with respect to the antenna, and the combinations represent the polarization on transmit and receive.

In order to support the development of PolSAR ship detection and classification capabilities for spaceborne PolSAR systems, simulated RADARSAT-2 products were used in this study to investigate the feasibility of improved ship detection and classification using polarimetric data. The RADARSAT-2 simulator (RSAT2SIMU) [2] simulates RADARSAT-2 products using data from the Environment Canada (EC) CV-580 C-band PolSAR in single look complex (SLC) form by increasing the noise floor and degrading the spatial resolution. The RSAT2SIMU simulator was developed by MDA and was made available to DRDC Ottawa by CSA. However, the simulator cannot simulate the geometry of the RADARSAT-2, such as the altitude, incidence angle and swath coverage. The simulated data quality depends on the quality of the input CV-580 data.

In this report, the polarimetric signatures of ships from simulated Fine Quad-Pol and Standard Quad-Pol Modes were studied. The input CV-580 data was obtained during the MARSIE trial [3].

1.1 Polarimetric data from the MARSIE trial

MARSIE trial is a “The Technical Cooperation Program (TTCP)”—lead activity that is exploring the benefits of sensor fusion to solve the target detection and tracking problem. The MARSIE trial was conducted in October 2005 off the East Coast of Canada and brought many sensors to bear on a set of known ship targets that were engaged in simulating a maritime incursion scenario (MIS).

The EC CV-580 polarimetric SAR was used as a proxy sensor for RADARSAT-2 polarimetry, as RADARSAT-2 was unavailable during the trial due to delays in its launch. MARSIE provided a unique opportunity to collect polarimetric SAR data for a variety of known ship types and sizes carrying out realistic manoeuvres.

In the recent report on the processing and analysis of polarimetric ship signatures from MARSIE trial for project Polar Epsilon [3], the results clearly demonstrated the significant improvement that may be realized by using polarimetric SAR for ship detection and potentially for ship classification.

This report provides a continuation of the MARSIE data analysis, focusing mainly on simulated RADARSAT-2 data by further analyzing the ships that were considered in [3].

1.2 Methodology

The polarimetric SAR data analysis includes target detection and target classification assessment, similar to those in [3]. The PolSAR ship detection algorithm used in this study was developed at DRDC Ottawa [4]. Three polarimetric decomposition methods were used: Pauli [5], Cameron [6] and SSCM [7]. The software for the Pauli and the Cameron methods was developed at DRDC Ottawa, while the SSCM software was implemented in a PolSAR workstation [9] that was developed at the CCRS and was made available to DRDC Ottawa by the CSA.

The main target used in the polarimetric analysis is the ship, *Dominion Victory*, which was imaged many times during the MARSIE trial. The *Dominion Victory* has a length of 25 m which matches the minimum detection criteria of Project Polar Epsilon. Two other ships from the MARSIE trial, *Gulf Service* and *HMCS Toronto*, were also studied. The lengths of these ships are 42 m and 134 m, respectively.

The detection performance is characterized by the receiver operating characteristic (ROC) which shows the probability of missed detection as a function of the probability of false alarm. The ROC analysis was performed for various radar systems, quadrature polarization, dual co-polarization (i.e., HH and VV) with both amplitude and phase, and HH single polarization.

The classification assessment consists of applying decomposition methods to the target images to determine which elemental scatterers from each method are present. Histograms of the distributions of elemental scatterers were studied for each decomposition method and each target.

For the Cameron and SSCM methods, the results were compared since both methods determine the maximum number of symmetric scatterers, such as trihedrals and dihedrals.

1.3 Outline of this document

The RADARSAT-2 capabilities and the RADARSAT-2 simulator are described in Sections 2 and 3, respectively. A brief overview of analysis methods is presented in Section 4. This is followed by a description of the polarimetric SAR data in Section 5 and the data analysis results in Section 6. A summary of the results, along with recommendations, is presented in Section 7. Many details have been relegated to Annexes including the simulated RADARSAT-2 ship images (Annex A), a catalogue of polarimetric decomposition results (Annexes B through E), and supporting photographic data (Annex F).

2. RADARSAT-2 Capabilities

The RADARSAT-2 modes of operation and swath coverage are illustrated in Figure 1 [1].

The Fine Beam Modes are intended for applications that require higher spatial resolution and that can be successful with narrower swath coverage. The Fine Beam Modes cover an incidence angle range from 30° to 41° . The incidence angle is the angle between the line of sight from the radar and the local vertical direction.

The Standard Beam Modes allow imaging over a wider range of incidence angles, from 20° to 49° . The Standard Beam Modes offer image quality characteristics that provide a compromise between spatial resolution, radiometric resolution, and swath coverage.

In this report, we focused on the Fine Quad-Pol Mode and the Standard Quad-Pol Mode. The key parameters of these two modes are summarized in Table 1.

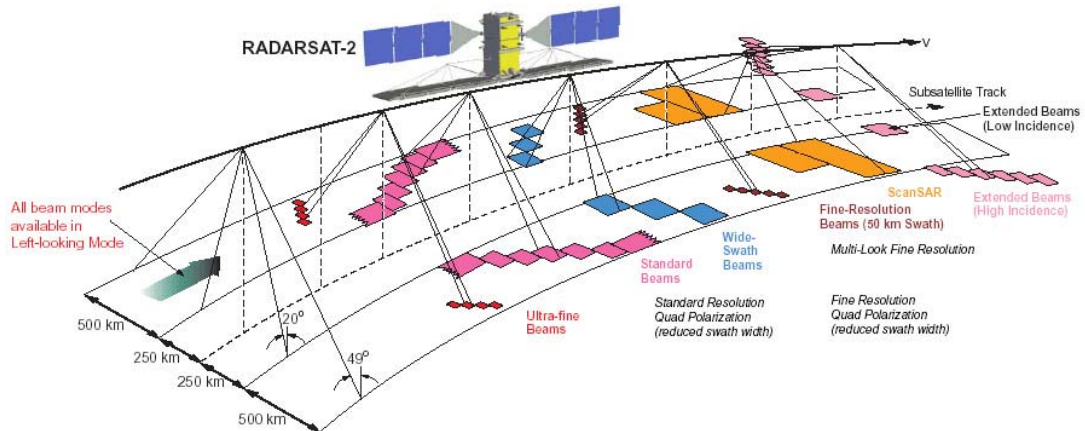


Figure 1: RADARSAT-2 operation modes and coverage (used with permission [1]).

Table 1: Key parameters of RADARSAT-2 polarimetric image modes.

Beam Mode		Nominal Incidence Angle, θ_{inc} ($^\circ$)	Nominal Swath Width (km)	Nominal Swath Coverage (km)	Approximate resolution GNDRg* \times Az (m)
Quad-Pol (HH, HV, VH, VV)	Fine	30 – 41	25 – 50	400 – 600	11 \times 9
	Standard	20 – 41	25 – 50	250 – 600	25 \times 28

* GNDRg: Ground range, AZ: Azimuth.

3. RADARSAT-2 simulator

The RADARSAT-2 Simulator, RSAT2SIMU, is intended to simulate images with the same resolution, pixel spacing and the noise equivalent sigma zero (NESZ) as RADARSAT-2 products starting from EC CV-580 PolSAR data [2].

3.1 Simulation process

The input data to the RSAT2SIMU is radiometrically calibrated EC CV-580 SLC data. The simulation of the RADARSAT-2 data from the CV-580 data involves three steps:

- Adding zero-mean complex Gaussian noise to increase NESZ to RADARSAT-2 levels;
- Degrading the spatial resolution by filtering in the slant range and azimuth directions to achieve the required resolution and spectral shapes, while preserving polarimetric information; and
- Re-sampling by interpolating in the slant-range and azimuth directions to achieve the required sample spacing.

The key system parameters of the CV-580 PolSAR sensor and RADARSAT-2 are compared for single look data in Table 2. The range sample spacing of RADARSAT-2 is calculated using different sampling rates for various modes, and in azimuth is 5 m, which is about 10 times larger than that of the CV-580. The range resolution is in slant range for the CV-580 and in ground range for RADARSAT-2. The slant range sample spacing listed in the table was obtained from the output header files of the simulated RADARSAT-2 images. Each polarimetric channel was processed separately using the same parameters. All four channels (HH, HV, VH, and VV) were processed for the polarimetric modes.

Table 2: Key system parameters for the CV-580 and RADARSAT-2 SARs.

		CV-580	RADARSAT-2	
			Quad Fine	Quad Standard
Frequency (GHz)		5.3		5.405
Altitude (km)		5 to 7		798
Azimuth resolution (m)		~1	9	28
Range resolution (m)	Slant-range	6		
	Ground-range		11	25
Azimuth sample spacing (m)		0.4		5.1
Slant range sample spacing (m)		4	4.7*	11.9*
NESZ (dB)		~ -40	-31	-28
Platform speed (m/s)		~140		7460

* According to the output header file of the simulated image.

RSAT2SIMU provides both a RADARSAT-2 product format and an intermediate product in CV-580 data format. In this report, the simulated RADARSAT-2 images in the CV-580 data format were used.

As an example, an input CV-580 image and the simulated RADARSAT-2 Fine Quad-Pol and Standard Quad-Pol Mode images in CV-580 format are illustrated in Figure 2 and Figure 3, respectively. This image includes an urban environment, residential areas, buildings, parks, bridges, bodies of water, etc. Figure 3a) and 3b) are intended to be illustrative of the simulated RADARSAT-2 Fine Quad-Pol and Standard Quad-Pol images from the CV-580 data.

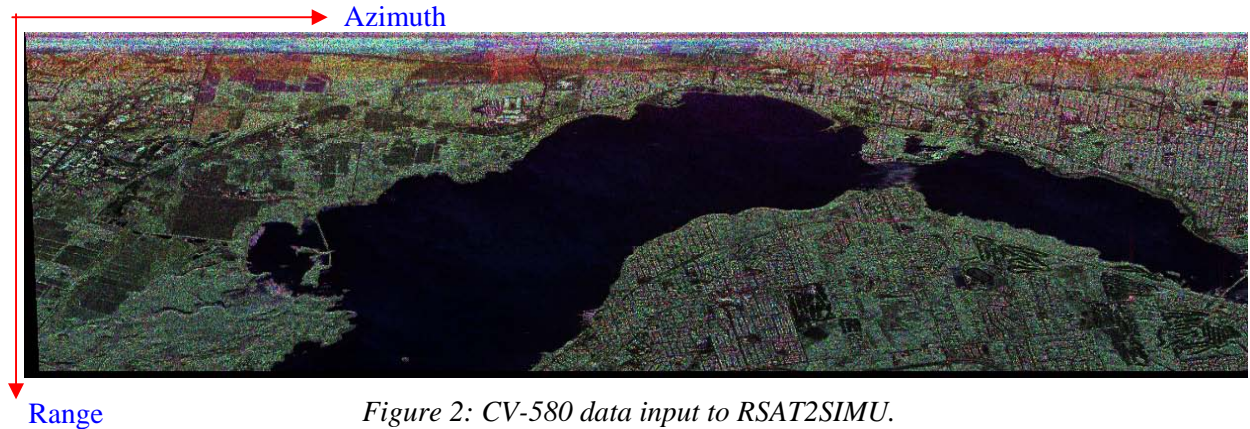


Figure 2: CV-580 data input to RSAT2SIMU.

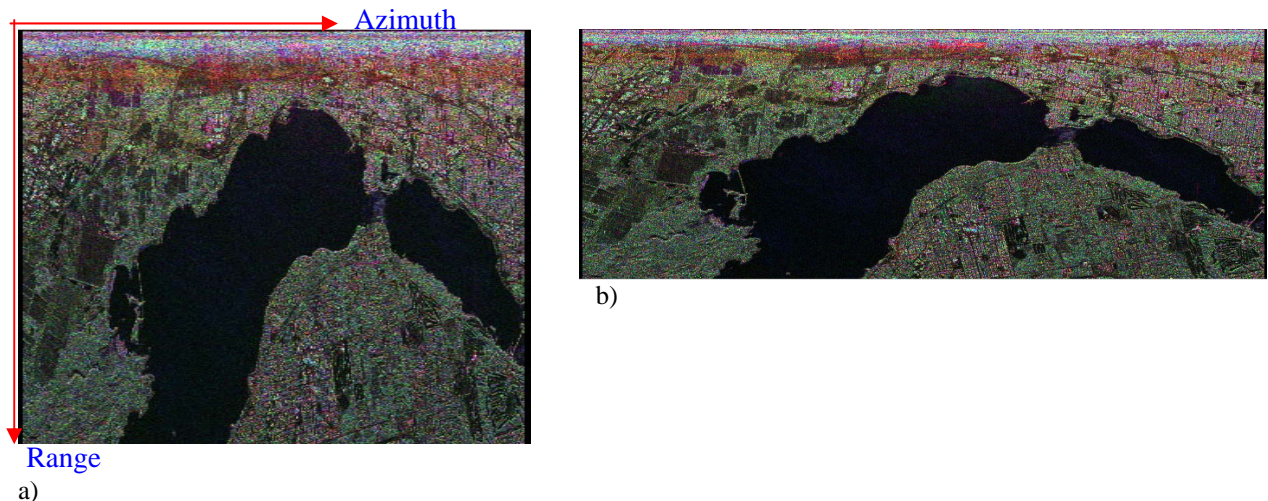


Figure 3: Simulated RADARSAT-2 images; a) Fine Quad-Pol Mode; b) Standard Quad-Pol Mode.

3.2 Differences with respect to RADARSAT-2 products

There are a number of differences between the simulated products and actual RADARSAT-2 products relevant to this study:

- The polarimetric SAR data quality has significant effects on the polarimetric signatures of the targets and the data quality depends largely on the various calibrations, such as

radiometric, phase and geometric calibration [17]. The simulated data quality is determined by the CV-580 calibration system and not the RADARSAT-2 calibration system;

- The NESZ is assumed constant over both the input and output images. In practice, NESZ varies over the swath, being lower at the centre of the swath and higher at the swath edges. This variation is caused by the antenna pattern of the sensor, which varies from beam to beam; and
- The simulated products do not represent a particular RADARSAT-2 beam. The CV-580 covers a wide range of incidence angles, far exceeding the incidence angle range of the RADARSAT-2 beams. CV-580 coverage is limited compared to that of RADARSAT-2. The size of the simulated region does not represent the size of a RADARSAT-2 product.

4. Overview of analysis methods

The polarimetric SAR data analysis includes ship detection and target classification assessment. For ship detection, we studied the detection performance of various PolSAR systems and estimated the receiver operating characteristic (ROC). The performance of three PolSAR system configurations was compared: polarimetric, dual co-polarization (i.e., HH and VV) with relative phase, and single polarization HH.

For target classification, three polarimetric decomposition methods were considered: Pauli, Cameron, and SSCM ([5], [6], [7]).

4.1 Receiver operating characteristic

The ROC is plotted as the probability of missed detection (P_{MD}) versus probability of false alarm (P_{FA}). Measured data processed by COASP [10] were used to calculate these probabilities using a well-known statistics-based methodology based upon likelihood ratio tests with the Neyman-Pearson criterion ([4],[11]).

A polarimetric SAR system provides observation of the scattering matrix $\mathbf{X}(i, j)$ for each pixel (i, j) in an image. The matrix components S_{HH} , S_{HV} , S_{VH} , and S_{VV} are complex valued elements, representing the scattering magnitude and phase for the possible combinations of horizontal (H) or vertical (V) transmit and receive polarizations. The components of $\mathbf{X}(i, j)$ can be written as a vector:

$$\mathbf{X}(i, j) = [S_{HH}(i, j) \quad S_{HV}(i, j) \quad S_{VH}(i, j) \quad S_{VV}(i, j)]^T \quad (1)$$

where the superscript T is the transpose operator.

Ship detection is a binary decision problem. The fundamental algorithms of PolSAR ship detection are based on statistical decision theory that may be applied directly to the components of the scattering matrix to obtain a decision variable. A likelihood ratio test with the Neyman-Pearson criterion is used to define a point detection criterion. The Gaussian distributions for scattering matrix components are assumed to derive an approximate decision variable, while the measured data may be used to calculate the detection variables.

Following [4], the decision variable is approximately given by

$$\mathbf{X}^H (C_o^{-1}) \mathbf{X} = \begin{cases} > \eta & \text{for a ship} \\ \leq \eta & \text{for ocean} \end{cases} \quad (2)$$

where C_o is the covariance matrix of the ocean.

For a polarimetric system, \mathbf{X} is given by Equation (1); for a dual co-polarization system, such as HH/VV with amplitude and phase, \mathbf{X} is given by

$$\mathbf{X}(i, j) = [S_{HH}(i, j) \quad S_{VV}(i, j)]^T \quad (3)$$

For a single polarisation system, the decision variable is given by the amplitude as

$$|X|^2 \left(\frac{1}{\sigma_o^2} \right) = \begin{cases} > \eta & \text{for a ship} \\ \leq \eta & \text{for ocean} \end{cases} \quad (4)$$

where σ_o^2 is the mean value of the ocean intensity. From these algorithms, we can see that a polarimetric system contains amplitude and phase information from four channels. As such, it is expected to provide the best detection performance compared to systems with fewer channels. A dual co-polarization system with amplitude and phase contains information from two channels, so it should provide better detection performance than a single channel system which contains only the amplitude information.

The detection performance is determined by two factors: the probability of false alarm (P_{FA}) and the probability of missed detection (P_{MD}). The ROC plots the probability of missed detection versus the probability of false alarm. Measured data is used to calculate these probabilities as the detection threshold η is varied.

The algorithms for calculation of the ROC can be applied to any designed probability of false alarm, such as $P_{FA} = 10^{-9}$, provided there are enough ocean samples available. The algorithms are independent of the environmental conditions; they can be applied to any sea state condition.

The accuracy of the estimated values of P_{MD} and P_{FA} may be determined from the number of missed detection and false alarm events. For a $P_{FA} = 10^{-9}$, to obtain an error of about 30% in the estimate of P_{FA} , roughly 10^{10} independent ocean samples at the same geometry and environmental conditions are required; to obtain an error of about 10%, roughly 10^{11} independent ocean samples are required. Since these numbers are rather large, $P_{FA} = 10^{-4}$ is used to estimate the relative performance, which for 10^6 ocean samples gives an error of 10%.

For target detection, several steps are required. In this study, the detection is performed on each pixel in the image and $P_{FA} = 10^{-4}$ is set for considerations of:

- Obtaining lower P_{MD} ; and
- Constraining the estimation accuracy due to the limited number of available samples.

There is a trade off between P_{FA} and P_{MD} . In general, the lower P_{FA} is set for detection, the higher P_{MD} will be. To obtain a lower P_{FA} with a lower P_{MD} , a combination of pixel detection with other algorithms must be employed. For example, following pixel-based detection, other algorithms such as target clustering, sub-aperture analysis, or polarimetric signature analysis may be applied to achieve a lower P_{FA} with a low P_{MD} . For clustering, the detected pixels must be grouped and a decision made as to whether or not there are sufficient pixels in the group to represent a target. Such a procedure will improve P_{FA} and P_{MD} , but at the cost of increasing the minimum size of target that can be detected. Phase interferogram analysis between the HV and VH channels in polarimetric systems can aid in distinguishing the targets from the ambiguities [12]. This will also reduce the P_{FA} .

4.2 Polarimetric target decomposition

4.2.1 Pauli

A linear polarization scattering matrix \mathbf{S} can be expressed in the Pauli basis [5] as:

$$\Psi_p = \left\{ \sqrt{2} \begin{bmatrix} 1 & 0 \\ 0 & 1 \end{bmatrix}, \sqrt{2} \begin{bmatrix} 1 & 0 \\ 0 & -1 \end{bmatrix}, \sqrt{2} \begin{bmatrix} 0 & 1 \\ 1 & 0 \end{bmatrix}, \sqrt{2} \begin{bmatrix} 0 & -i \\ i & 0 \end{bmatrix} \right\} \quad (5)$$

This representation permits the extraction of physical information from the 2×2 coherent scattering matrix. Under the reciprocity assumption (i.e., $S_{HV} \cong S_{VH}$), the Pauli scattering vector is given by [5]:

$$k = \frac{1}{\sqrt{2}} [S_{HH} + S_{VV} \quad S_{HH} - S_{VV} \quad S_{HV} + S_{VH}]^T \quad (6)$$

In Pauli decomposition analysis, each pixel is assigned to one of three classes, depending on which of the components is the largest in amplitude. For class 1, $(S_{HH} + S_{VV})$ is the largest, representing single or odd bounce scattering; for class 2, $(S_{HH} - S_{VV})$ is the largest representing double or even bounce scattering; and for class 3, $(S_{HV} + S_{VH})$ is the largest representing volume scattering.

The physical interpretation of three basic scattering mechanisms is illustrated in Figure 4.

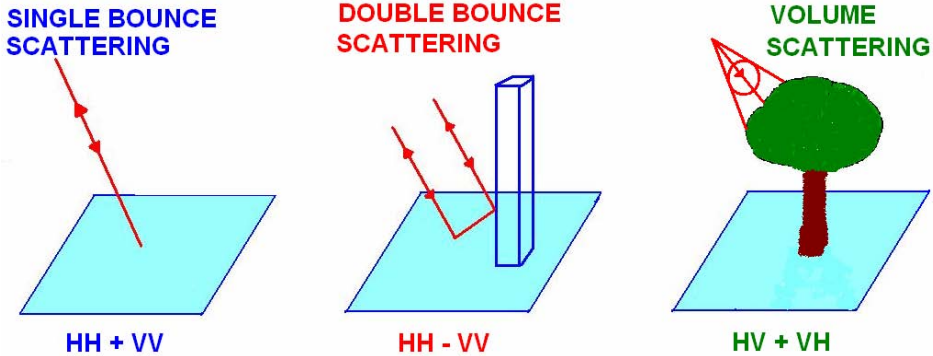


Figure 4: Physical interpretation of three basic scattering mechanisms.

4.2.2 Cameron

In the Cameron method [6], the measured scattering matrix is decomposed based on two basic properties of radar returns: reciprocity and symmetry. An arbitrary scattering matrix could be coherently decomposed into a nonreciprocal component, a maximum symmetric component, and a minimum symmetric component. In this report, only the maximum symmetric scattering components are studied. These components are trihedral, diplane (i.e., dihedral), dipole, cylinder,

narrow diplane, and quarter-wave devices. The symmetric scatterers are represented on a Unit disk as shown in Figure 5.

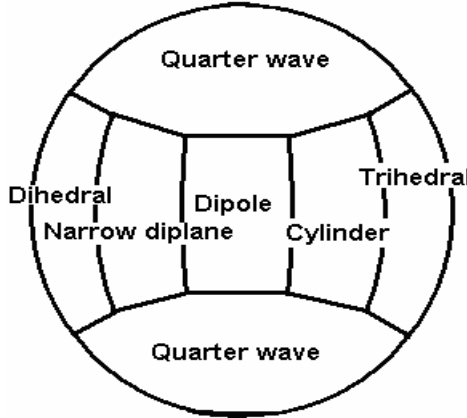


Figure 5: Unit disk representation of symmetric scatterers.

A symmetric scatterer can be represented in terms of its normalized diagonal scattering matrix $\Lambda(z)$:

$$\Lambda(z) = \frac{1}{\sqrt{1+|z|^2}} \begin{pmatrix} 1 \\ 0 \\ 0 \\ z \end{pmatrix} \quad |z| \leq 1 \quad (7)$$

where the parameter z determines the scatterer type associated with a particular scattering matrix, which can be represented by a point in the unit disc of the complex plane. The six elemental scatterers are expressed in terms of $\Lambda(z)$ as follows:

trihedral	diplane/ dihedral	dipole	cylinder	narrow diplane	quarter wave
$\Lambda(1)$	$\Lambda(-1)$	$\Lambda(0)$	$\Lambda(\frac{1}{2})$	$\Lambda(-\frac{1}{2})$	$\Lambda(\pm i)$

Each pixel is then assigned to one of six classes, depending on which of the components is the shortest distance d away, according to the symmetric scatter distance measure:

$$d(z_1, z_2) = \cos^{-1} \left[\frac{\max(|1+z_1 z_2^*|, |z_1 + z_2^*|)}{\sqrt{1+|z_1|^2} \sqrt{1+|z_2|^2}} \right], \quad 0 \leq d \leq \frac{2}{\pi} \quad (8)$$

where z_1 and z_2 are the z values for the two scatterers under consideration. In general, trihedral represents odd bounce scattering and diplane represents even bounce scattering, as in the Pauli decomposition. Also, cylinder represents curved metallic plates as well as large diameter or pipe-like objects.

4.2.3 Symmetric Scattering Characterization Method

The SSCM is another approach to exploit the information from the largest target symmetric scattering components [7]. These components are the same as those defined in the Cameron method.

The symmetric scattering vectors in SSCM are represented in terms of the latitude 2ψ and longitude 2χ on a target Poincaré sphere surface, as shown in Figure 6, instead of on the Unit Disk considered in the Cameron method. The coordinates of the six largest target symmetric elemental scatterers on the Poincaré sphere are summarized in Table 3.

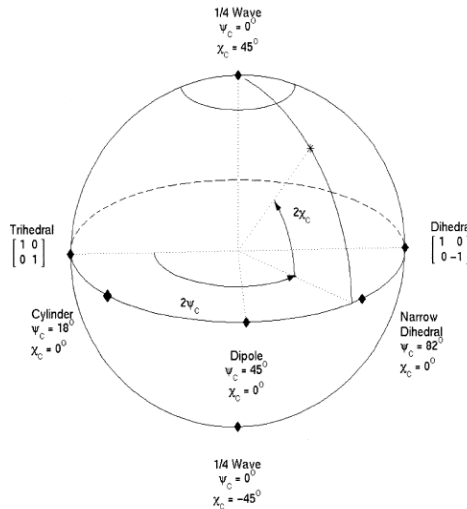


Figure 6: Poincaré sphere representation of symmetric scatterers (use with permission [7]).

Table 3. Elemental scatterer coordinates on the Poincaré sphere.

scattering	trihedral	dihedral	dipole	cylinder	narrow diplane	quarter wave
(ψ_c, χ_c)	$(0^\circ, 0^\circ)$	$(90^\circ, 0^\circ)$	$(45^\circ, 0^\circ)$	$(18.43^\circ, 0^\circ)$	$(81.88^\circ, 0^\circ)$	$(0^\circ, 45^\circ)$

Based on the symmetric scatterer centre on the Poincaré sphere, six symmetric scatterers can also be generated by using the thresholds shown in Table 4.

For example, a symmetric scatterer is classified as a trihedral scatterer if its Poincaré sphere longitude angle ψ_c is between 0° and 9.22° and its Poincaré sphere latitude angle χ_c is between -12.5° and $+12.5^\circ$.

Table 4: threshold to generate each symmetric scatterer.

symmetric scatterer	ψ_c ($^\circ$)		χ_c ($^\circ$)
trihedral	0 to 9.22	and	-12.5 to 12.5
cylinder	9.22 to 31.72		
dipole	31.72 to 63.44		
narrow diplane	63.44 to 85.94		
dihedral	85.94 to 90		
quarter wave	0 to 90		< -12.5 or > 12.5

5 Polarimetric SAR data

5.1 Data description

The PolSAR data used in this report are listed in Table 5. They were obtained during the MARSIE [3] and the Urban PolInSAR [14] trials using the EC CV-580 PolSAR sensor.

Table 5: CV-580 data used in the RADARSAT-2 simulations.

Flight line/pass, date	Sensor look direction	Trial name
11p8, 04-Sep-02	left	Urban PolInSAR
141p1, 20-Oct-05	Right	MARSIE
141p2, 20-Oct-05	Left	MARSIE
141p3, 20-Oct-05	Right	MARSIE
142p4, 20-Oct-05	left	MARSIE
122p2, 17-Oct-05	left	MARSIE

The Urban PolInSAR trial data were processed using the Configurable Airborne SAR Processor (COASP) since the targets of interest in this image are static targets. However, the individual ship images from the MARSIE trial were reprocessed using the Chip-based Adaptive SAR Processor (CHASP) to improve the ship focus by compensating for the ship motion. Both processors, COASP and CHASP, were developed at DRDC Ottawa [10].

The Urban PolInSAR data were used to evaluate the quality of the simulated data, while the main targets used in the polarimetric analysis are vessels which were obtained during the MARSIE trial, as listed in Table 6. The length of the *Dominion Victory* matches the minimum detection criteria of project Polar Epsilon; it was imaged several times from various incidence and aspect angles. The aspect angle is the angle from the orientation of the ship to the Azimuth direction (clockwise).

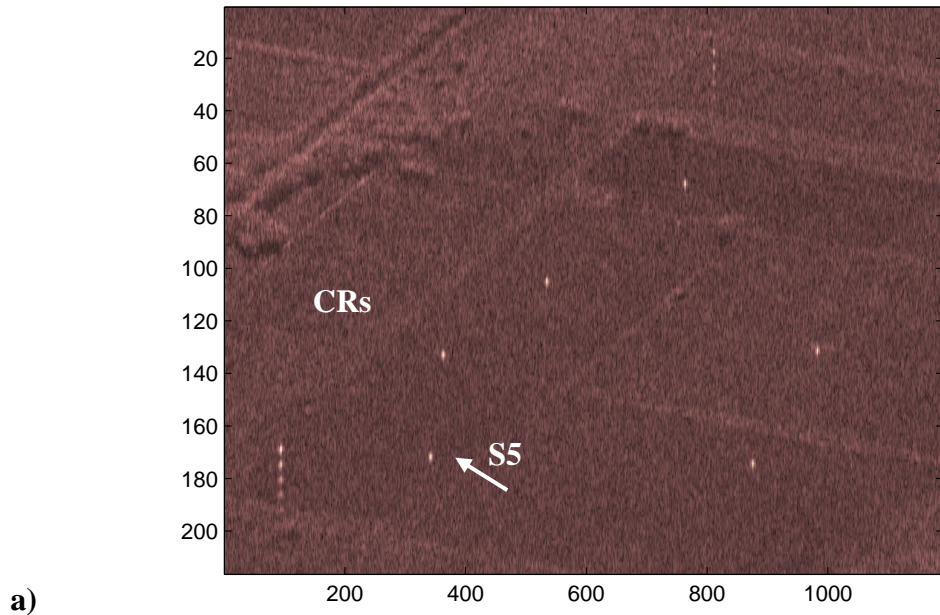
Table 6: Ships used in the analysis

Ship	Length (m)	Type
<i>Dominion Victory</i>	25	Multi-purpose support
<i>Gulf Service</i>	42	Tug
<i>HMCS Toronto</i>	134	Halifax Class Patrol Frigate

5.2 Data quality evaluation

In order to evaluate the quality of simulated RADARSAT-2 data, a known corner reflector (CR), referred to as S5 and deployed at the Cannaught Range calibration site in the Ottawa area, was studied. The HH images of the calibration site from the CV-580 and simulated RADARSAT-2 Fine Quad-Pol and Standard Quad-Pol Modes are shown in Figure 7. The CV-580 image was obtained from flight line 1 pass 8 (11p8) during the Urban PolInSAR trial. Corner reflector S3 has a 70.5 cm back spine length.

Since the HH channel image from RADARSAT-2 should be similar to a RADARSAT-1 image, a RADARSAT-1 image obtained from 7 May 2004 is shown in Figure 8 as a comparison. In addition, a corner reflector having a back spine length of 75 cm, located at N45.37368 and W75.92441 in the image, was analyzed; the results were compared to those from the simulated data since these CRs have similar size. This image is a Fine 2 Near beam mode with a nominal resolution of 9 m in ground range and 9 m in azimuth, acquired in the ascending pass direction [15].



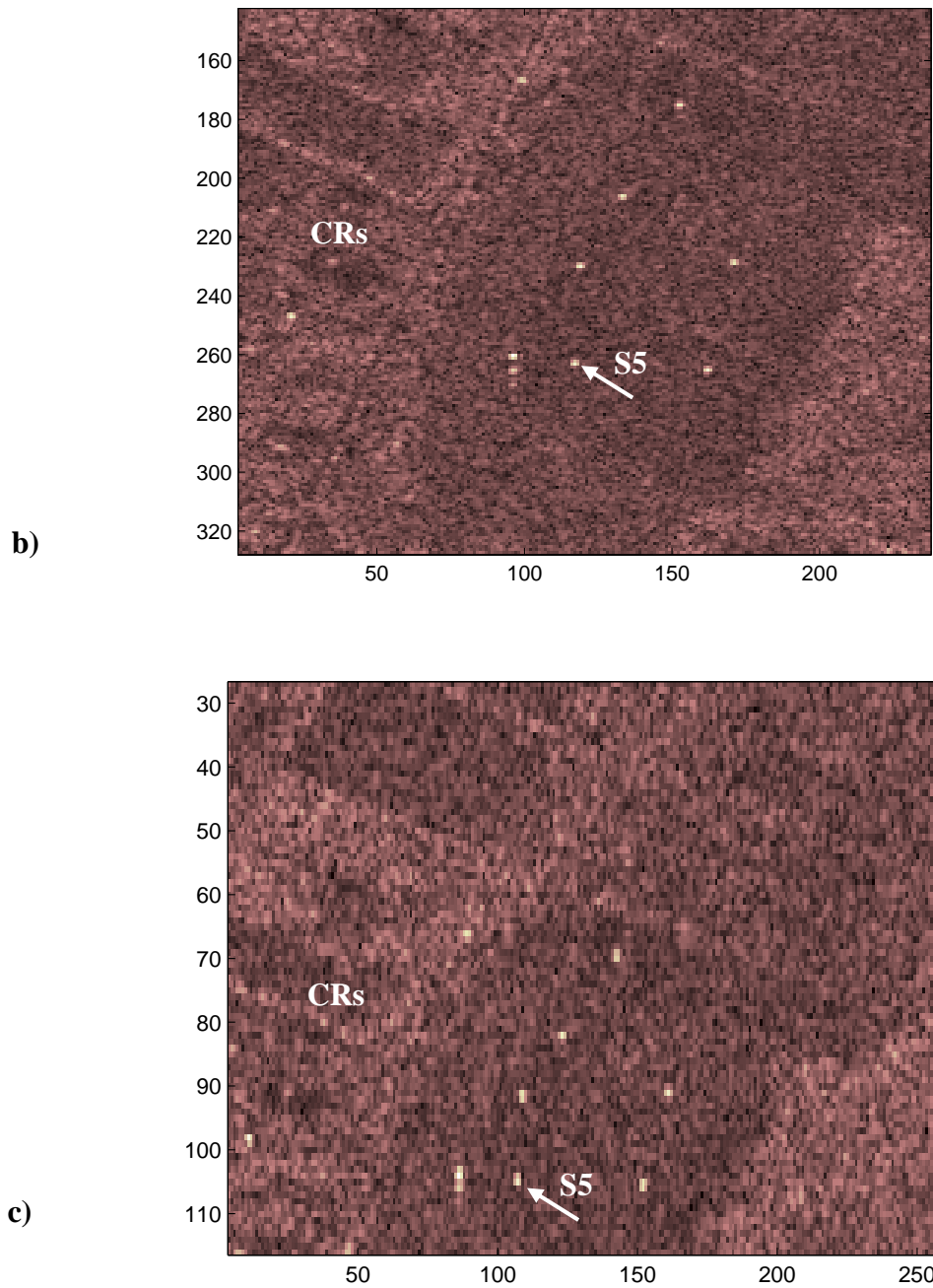


Figure 7: Corner reflectors and calibration site in HH images (l1p8, 24 September 2002); a) CV-580; b) simulated RADARSAT-2 Fine Quad-Pol Mode; c) simulated RADARSAT-2 Standard Quad-Pol Mode.

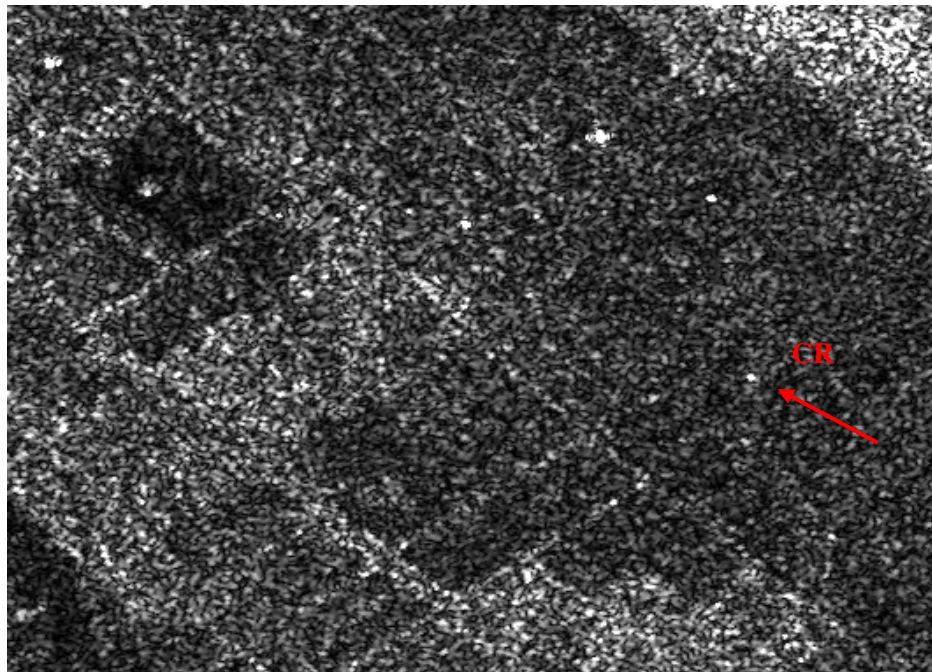


Figure 8: Calibration site and 75 cm corner reflector in a RADARSAT-1 image (7 May 2004).

The analysis results, such as peak value, mean clutter value, peak-to-clutter ratio (PCR), and resolutions derived from the -3dB “width” response of the CR, for the various modes are summarized in Table 7. The target peak to clutter ratio (PCR) of Standard Quad-Pol Mode simulated RADARSAT-2 HH data is almost the same as that of actual RADARSAT-1 data, but the simulated Fine Quad-Pol Mode PCR is much higher.

The simulated RADARSAT-2 product co-pol and cross-pol channels are also compared. The HH and VV corner reflector measurements results are similar while HV and VH responses are much lower.

The resolutions of the simulated RADARSAT-2 images in the azimuth direction are comparable to the actual resolution (see Table 1). It is worth noting that the azimuth resolution of 28 m (see Table 1) in the actual RADARSAT-2 Standard Quad-Pol Mode is for 4-looks. However, the azimuth resolution of the simulated products is for one-look (see Table 7). The range resolution of the simulated images can not be compared to the actual products since the range represents the slant range in the simulated data, but represents the ground range in the actual data.

Table 7: Statistical parameters of a corner reflector and the image resolution.

S5			Peak (dB)	Mean Clutter (dB)	PCR (dB)	Resolution (m)
CV-580		HH	16.40	-17.99	34.39	6×1 , Slant Range \times AZ*
Simulated RADARSAT-2	FQ*	HH	6.54	-18.48	25.02	5.88×8.92 , Slant Range \times AZ
	StdQ*	HH	3.23	-17.57	20.80	14.63×9.59 , Slant Range \times AZ
RADARSAT-1		HH	8.38	-11.90	20.28	9 X 9, Ground Range \times AZ
Simulated RADARSAT-2	FQ	VV	5.36	-18.59	23.95	
	StdQ	VV	2.01	-18.54	20.56	
Simulated RADARSAT-2	FQ	HV	-15.11	-23.99	8.88	
	StdQ	HV	1.55	-25.47	27.01	
Simulated RADARSAT-2	FQ	VH	-13.83	-24.59	10.76	
	StdQ	VH	1.07	-25.52	26.59	

* FQ: Fine Quad-Pol Mode, StdQ: Standard Quad-Pol Mode, AZ: Azimuth.

Furthermore, an urban image, consisting of buildings, streets, bridges, parks, etc., was also studied. The images from the HH channel of simulated RADARSAT-2 Fine Quad-Pol and Standard Quad-Pol Modes and RADARSAT-1 are shown in Figure 9 and Figure 10, respectively. In order to compare these images, the simulated RADARSAT-2 images are flipped vertically due to the different acquisition geometry.

The urban structures observed in the simulated RADARSAT-2 images are similar to those in the RADARSAT-1 image. However, the simulated RADARSAT-2 images will differ from actual images, as discussed in Section 3.2.

From these analysis results, the simulated RADARSAT-2 images are considered to be sufficient for the evaluation of the application of polarimetric SAR analysis algorithms developed using airborne PolSAR data to spaceborne systems, specifically for ship detection and target classification methods.

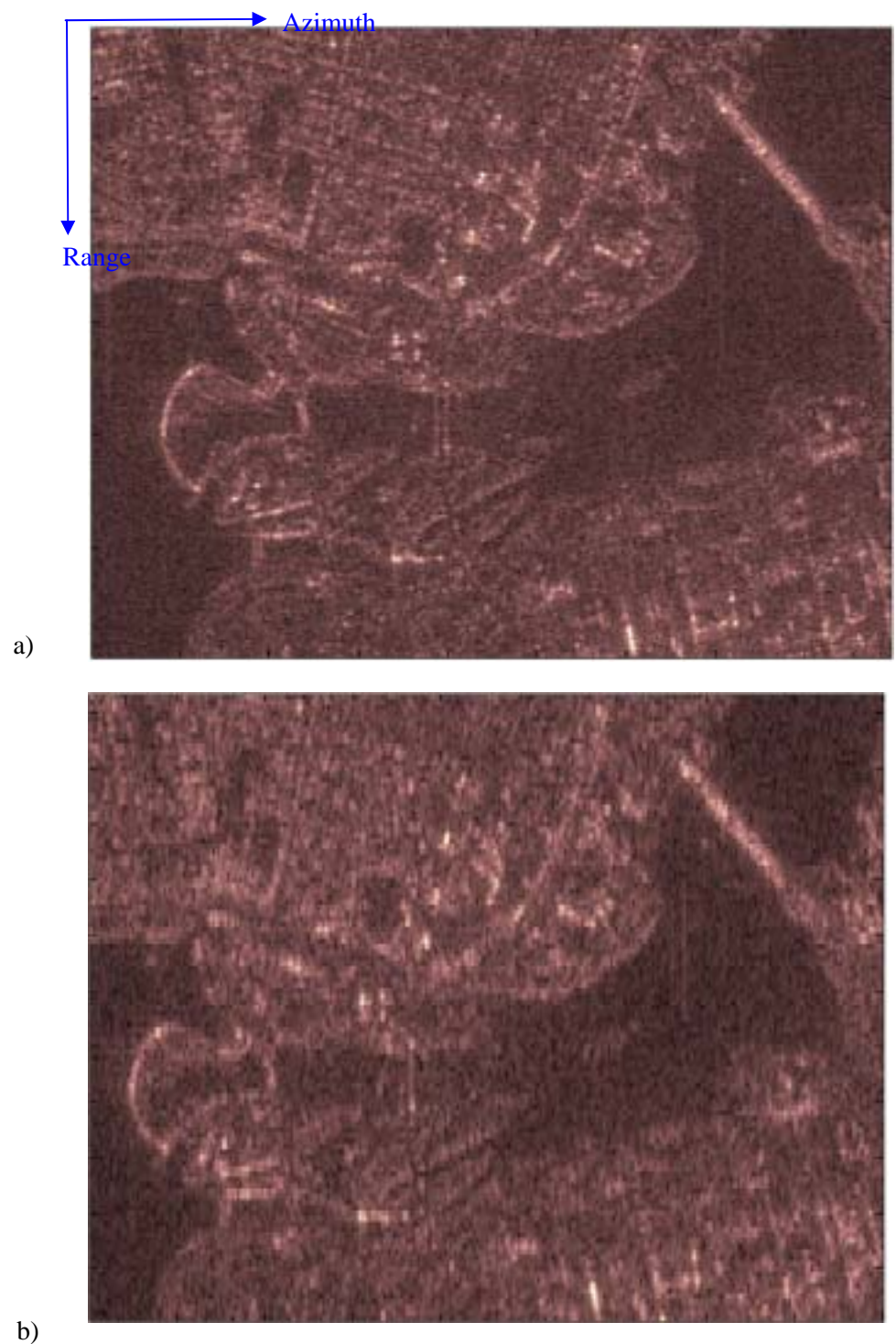


*Figure 9: Simulated RADARSAT-2 images of urban environment (l1p8, 24 September 2002);
a) Fine Quad-Pol Mode; b) Standard Quad-Pol Mode.*

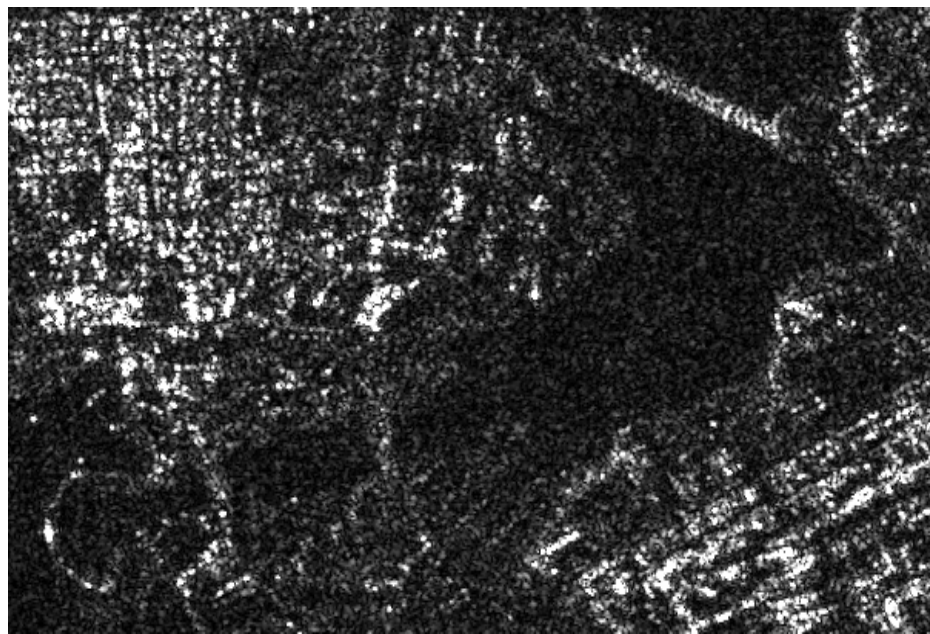


Figure 10: RADARSAT-1 image of urban environment (7 May 2004).

6 Analysis results

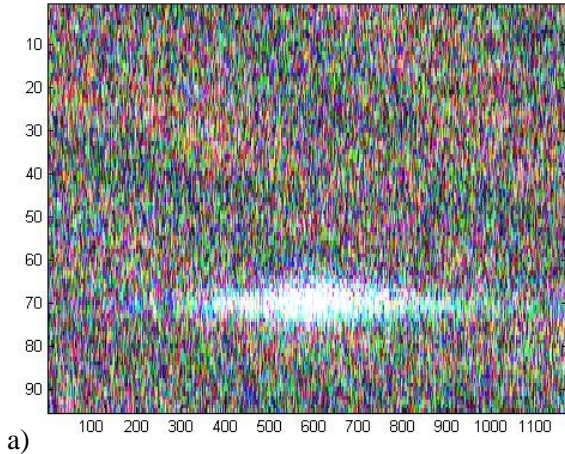
The polarimetric SAR data analysis includes target detection and target classification assessment. The target detection performance is estimated using the ROC curve and the classification is carried out using three polarimetric decomposition methods and the target signature analysis.

For ROC analysis, the standard PolSAR processed data were used. However, the most standard PolSAR processed ships are smeared due to ship motion. Therefore, for target classification analysis, the individual ships were reprocessed to improve the focus before RADARSAT-2 simulation.

Examples of the analysis results of the *Dominion Victory* from l41p1 are presented in this Section; more results can be found in Annexes A through E.

6.1 Simulated vessel images

An example of a CV-580 CHASP-processed image and the simulated RADARSAT-2 Fine Quad-Pol Mode and Standard Quad-Pol Mode images are shown in Figure 11. The ship is visible in both simulated RADARSAT-2 images. However, in l41p2, the ship doesn't appear in the simulated images (See Annex A).



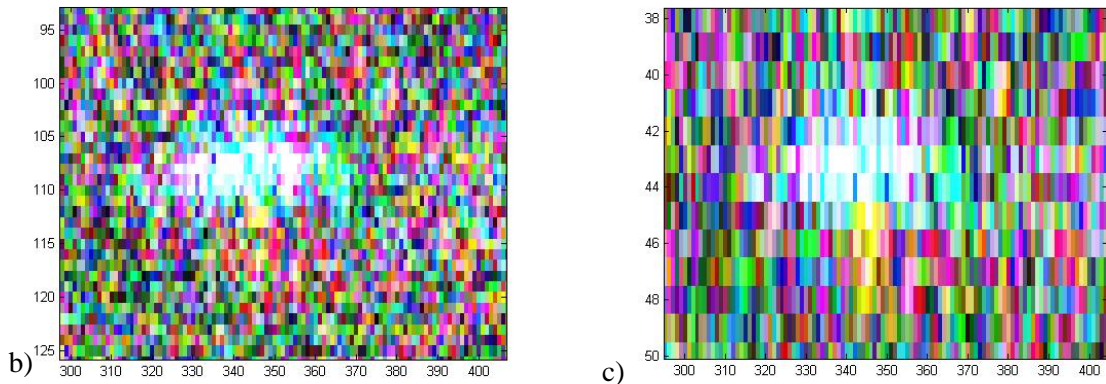


Figure 11: Polarimetric image of Dominion Victory (l41p1, 20 October 2005); a) CV-580; b) simulated RADARSAT-2 Fine Quad-Pol Mode; c) simulated RADARSAT-2 Standard Quad-Pol Mode.

6.2 Receiver Operating Characteristic

The detection performance was estimated for three systems, polarimetric, dual co-polarization with amplitude and phase, and single channel HH. The results are shown in Figure 12.

The advantage of a quad polarimetric system is apparent (i.e., decreased probability of missed detection, decreased probability of false alarm), which uses the available amplitude and phase information (triangles), in both Find Quad-Pol and Standard Quad-Pol Modes. The dual co-polarization system with phase (circles) provides better detection performance than a single channel HH polarization system (asterisks). In principle, a dual polarization system should provide wider swath coverage than a quad polarimetric system. This performance improvement as polarimetric channels are added has been demonstrated previously (see [3], [4] and Annex B).

The variability in ship detection of various systems is also shown in Figure 12a. For this example, the Fine Quad-Pol Mode had an ocean sample composed of 630,000 pixels and a ship sample composed of 160 pixels, while the Standard Quad-Pol Mode had an ocean sample of 227,000 pixels and ship sample composed of 96 samples. The available number of ocean samples depends on the maximum data size that can be handled by the simulator, while the maximum number of ship samples depends on the size of the ship and the sample spacing of the RADARSAT-2 data.

By arbitrarily selecting a probability of false alarm of $P_{FA} = 10^{-4}$, the relative improvement in ship detectability may be quantified by comparing the probability of missed detection P_{MD} across the cases studied. The relative improvement in the detection performance of all three images from 20 October 2005 is summarized in Table 8 by taking the ratio of the observed P_{MD} to that of polarimetry P_{MD}^Q . In Table 8, entries where no number is given indicates no detection. From Table 8, we can see that in some cases, *Dominion Victory* could not be detected using a single channel system. Furthermore, it could not always be detected even when using a dual co-pol system. The probability of missed detection is often high for single channel and dual-polarized

systems. The results demonstrate that the polarimetric system is always the best. The dual co-polarized HH-VV system provides better detection than a single channel HH polarization system.

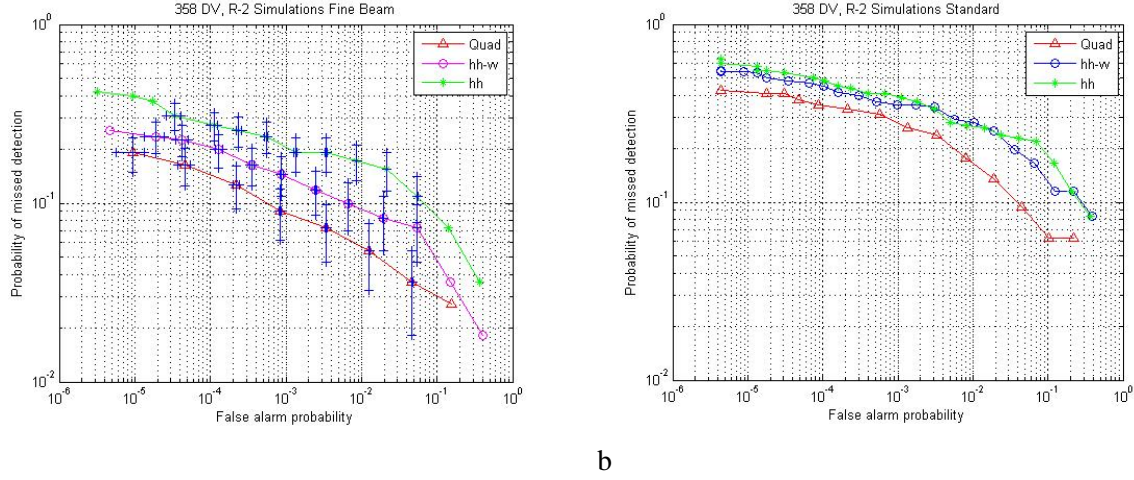


Figure 12: Detection performance for Dominion Victory (l41p1, 20 October 2005). a) Fine Quad-Pol Mode; b) Standard Quad-Pol Mode.

Table 8: Values of P_{MD} for $P_{FA} = 10^4$ for Dominion Victory.

		Dominion Victory (L=25m)			
line/pass		Find Quad-Pol		Standard Quad-Pol	
		P_{MD}^Q	P_{MD}/P_{MD}^Q	P_{MD}^Q	P_{MD}/P_{MD}^Q
l41p1 20-Oct-05	Quad P_{MD}	0.15	1.00	0.34	1.00
	HH-VV P_{MD}	0.22	1.47	0.45	1.32
	HH P_{MD}	0.28	1.87	0.49	1.44
l41p2 20-Oct-05	Quad P_{MD}	0.23	1.00	0.60	1.00
	HH-VV P_{MD}	-	-	0.70	1.17
	HH P_{MD}	-	-	-	-
l42p4 20-Oct-05	Quad P_{MD}	0.38	1.00	0.56	1.00
	HH-VV P_{MD}	0.49	1.29	-	-
	HH P_{MD}	0.70	1.84	-	-

6.3 Target decomposition

The three target decomposition methods, Pauli, Cameron and SSCM, were applied to the simulated RADARSAT-2 data. For the Pauli and Cameron decomposition analysis, a threshold for each ship was selected based on the estimated mean ocean clutter value (σ^o) to reduce the clutter in the decomposition results. The thresholds are listed in Table 9.

Table 9: Decomposition analysis thresholds.

Line/Pass	Ship Name	Reference Channel	Threshold (dB) Fine Quad-Pol and Standard Quad-Pol
17 Oct. 2005			
L22p2 (a342)	<i>Gulf Service</i>	HH	-15
l22p2 (a342)	<i>HMCS Toronto</i>	HH	-20
20 Oct. 2005			
l41p1 (a358)	<i>Dominion Victory</i>	HH	-15
l41p3 (a360)	<i>Dominion Victory</i>	HH	-12
l42p4 (a361)	<i>Dominion Victory</i>	HH	-14

6.3.1 Pauli

The Pauli decomposition results are shown in Figure 13, in which each pixel is assigned to one of three classes, depending on which of the components has the largest amplitude. For Class 1, $(S_{HH} + S_{VV})$ is the largest, for class 2, $(S_{HH} - S_{VV})$ is the largest, and for class 3, $(S_{HV} + S_{VH})$ is the largest. Class 1 represents odd bounce (blue), Class 2 represents even bounce (red), and the class 3 represents volume scattering (green). As might be expected, the ship image includes mainly double bounce scattering and single bounce scattering due to ship structure. Volume scattering also appears in the ship image in some cases. This may be due to multiple bounces from the ship structure or may be caused by uncompensated ship motion during image acquisition and processing.

It is noted that there are more single bounce scattering components in the simulated images than in the original CV-580 images ([3]).

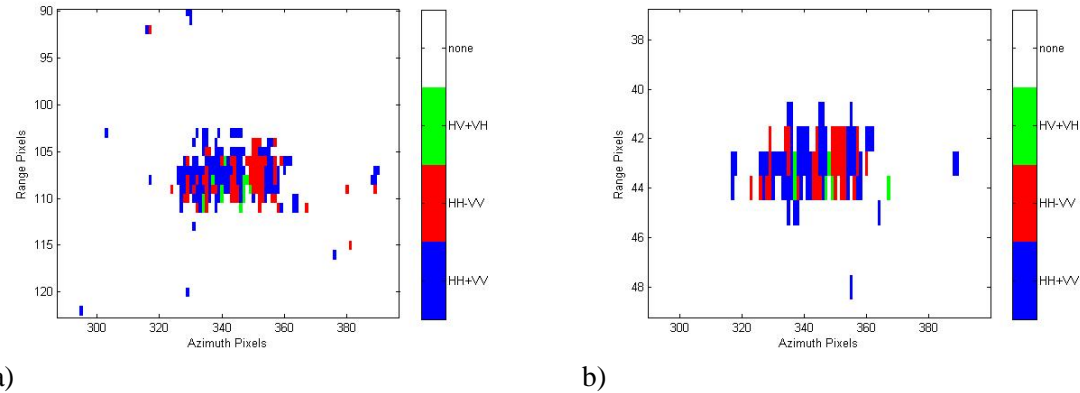


Figure 13: Pauli decomposition images of *Dominion Victory* (l41p1 20 October 2005). a) Fine Quad-Pol Mode; b) Standard Quad-Pol Mode.

6.3.2 Cameron

The Cameron decomposition results are shown in Figure 14. The ship image has been decomposed into six elemental scatterers. In this image, the most dominant component is the cylinder-like scatter, followed by the dipole and the quarter-wave device. The distribution of each component is shown in the histogram. The types of elemental scatterers are indicated as follows: 1: none classified, 2: trihedral, 3: diplane (i.e. dihedral), 4: dipole, 5: cylinder, 6: narrow diplane and 7: quarter-wave device.

For the cases studied, the dominant component varies. However, the distribution of dominant components from the Standard Quad-Pol Mode is similar to those from the Fine Quad-Pol Mode. The fractions of each elemental scatterer from the Cameron decomposition are summarized in Table 10 and Table 11. This report has focused on the distributions of numbers of elemental scatterers in the target displayed as a histogram. The distribution of scatterers is potentially useful for ship classification. But it is recommended to combine this information with other target analysis methods. It is judged that these distributions are not always different enough to permit clear classifications. Therefore, the use of the spatial distributions of scatterers should also be investigated.

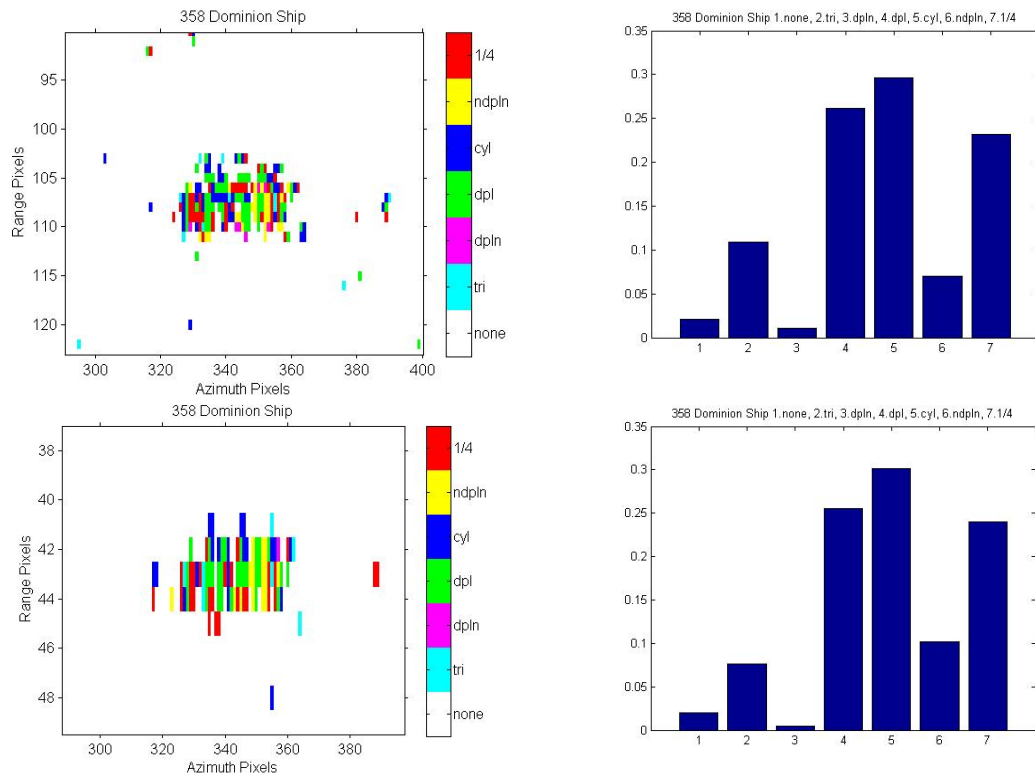


Figure 14: Cameron decomposition image (left) and histogram (right) of Dominion Victory (I41p1 20 October 2005). Top: Fine Quad-Pol, Bottom: Standard Quad-Pol. In the histograms (right): the scatterer type is along the x-axis and the percentage of the distribution is along the y-axis.

Table 10: Summary of elemental scatterer distributions for Cameron decomposition for simulated Fine Quad-Pol images.

Ship name	trihedral	diplane	dipole	cylinder	narrow diplane	quarter wave
17 Oct. 2005, l22p2 (a342)						
<i>Gulf Service</i>	0.1811	0.0157	0.0728	0.2953	0.0296	0.4055
<i>HMCS Toronto</i>	0.0386	0.0289	0.3269	0.2251	0.1715	0.2090
20 Oct. 2005, Dominion Victory						
l41p1 (a358)	0.1114	0.0107	0.2672	0.3023	0.0718	0.2366
l41p3 (a360)	0.6824	0.0011	0.0123	0.2783	0.009	0.0168
l42p4 (a361)	0.5557	0.0025	0.0164	0.3873	0.0050	0.0329

Table 11: Summary of elemental scatterer distributions for Cameron decomposition for Standard Quad-Pol images

Ship name	trihedral	diplane	dipole	cylinder	narrow diplane	quarter wave
17 Oct. 2005, l22p2 (a342)						
<i>Gulf Service</i>	0.2509	0.0215	0.0287	0.2616	0.0322	0.4051
<i>HMSC Toronto</i>	0.0544	0.0544	0.2646	0.2840	0.1790	0.1634
20 Oct. 2005, Dominion Victory						
l41p1 (a358)	0.0781	0.0052	0.2604	0.3073	0.1041	0.2448
l41p3 (a360)	0.7545	0.0120	0.0239	0.1976	0	0.0120
l42p4 (a361)	0.5849	0.0018	0.0055	0.3894	0.0018	0.0166

6.3.3 SSCM

The SSCM results are presented in term of the Poincaré sphere angles, longitude 2ψ and latitude 2χ , in Figure 15. A ship is decomposed into six elemental scatterers, as in the Cameron method. A representative SSCM result presented in terms of six types of symmetric scatterers is shown in Figure 16 and the distribution of each component is shown in the histogram. The types of elemental scatterers are indicated as follows: 1: trihedral, 2: diplane (i.e. dihedral), 3: dipole, 4: cylinder, 5: narrow diplane and 6: quarter-wave device.

The results for the cases considered are presented in Table 12 and Table 13.

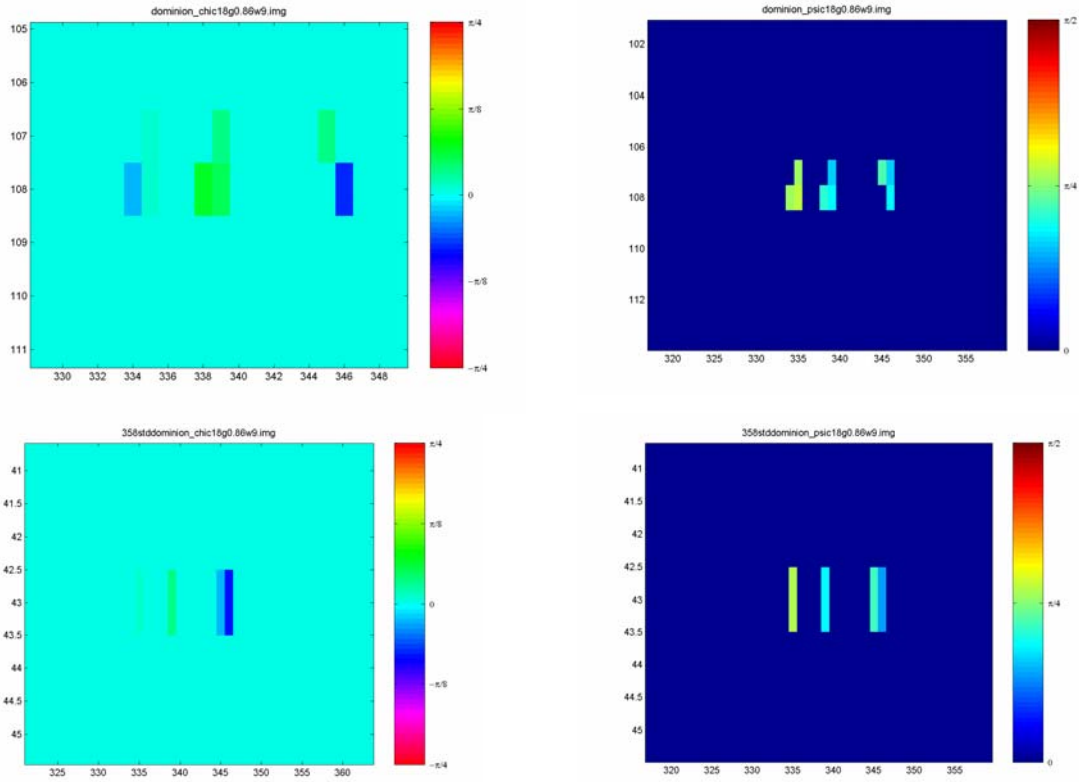


Figure 15: SSCM decomposition images of Dominion Victory (l41p1, 20 October 2005). Top: Fine Quad-Pol Mode; bottom: Standard Quad-Pol Mode. Left: Latitude coordinate; right: Longitude coordinate. Azimuth pixels are along the x-axis and range pixels are along the y-axis.

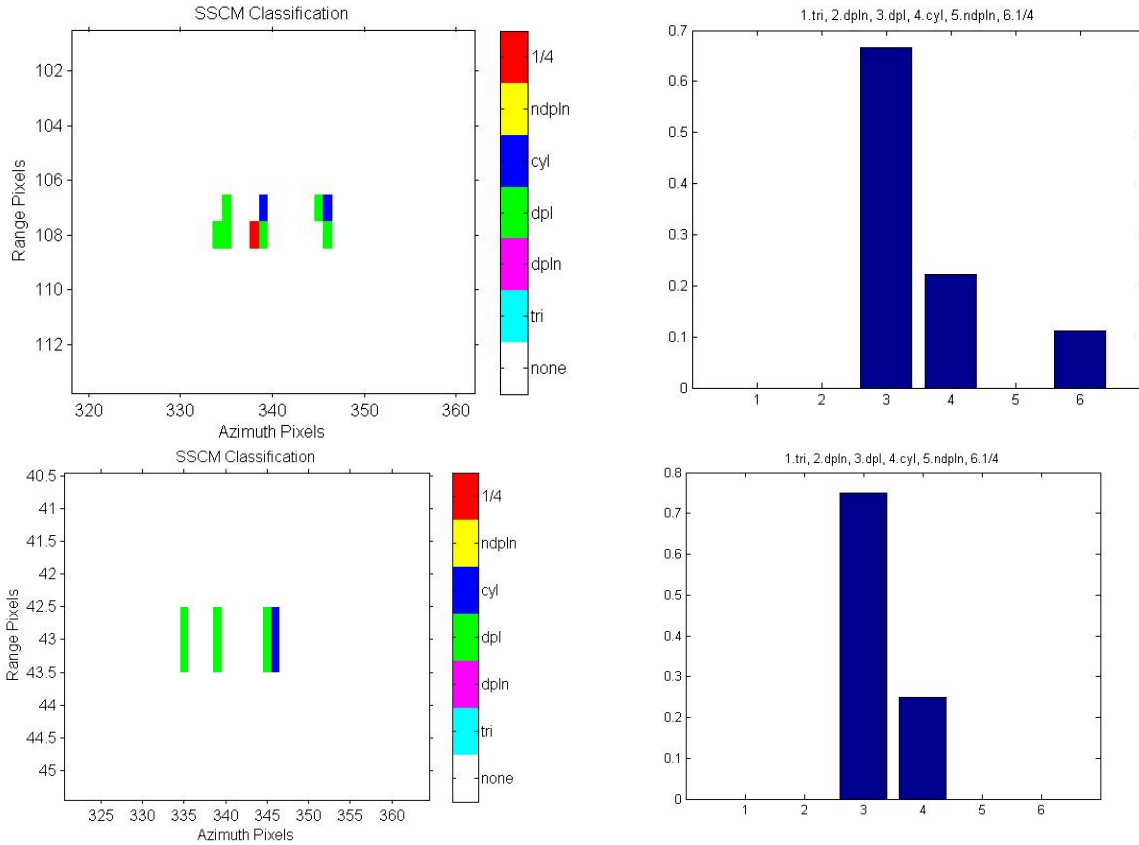


Figure 16: SSCM classification image (left) and histogram (right) of Dominion Victory (l41p1, 20 October 2005). Top: Fine Quad-Pol Mode; bottom: Standard Quad-Pol Mode.

In the histograms (right): the scatterer type is along the x-axis and the percentage of the distribution is along the y-axis.

In the SSCM analysis, the assessment method of scattering coherence of the target is different from that of the Cameron method. The scattering coherence must be tested before classification. For the cases studied, the target was tested as the coherent target in only three images; the classification results are not very promising since many elemental scatterers can not be classified. This may be due to the coarse resolution. Therefore, additional examples from a 134 m long ship, *HMCS Toronto*, are given in Figure 17 and Figure 18. The results are similar to those from the Cameron method (Annex D). This method may not be sufficient for small ship classification, however, it can be applied to large ships. The SSCM first finds the coherent scatterers and then classifies them. This results in a small number of classified pixels of small ships (See Figure 15 and 16). The amount of information generated by SSCM in these cases is not sufficient for ship classification. On the other hand, for large ships, the SSCM produces an acceptable number of classified pixels (See Figure 17 and 18).

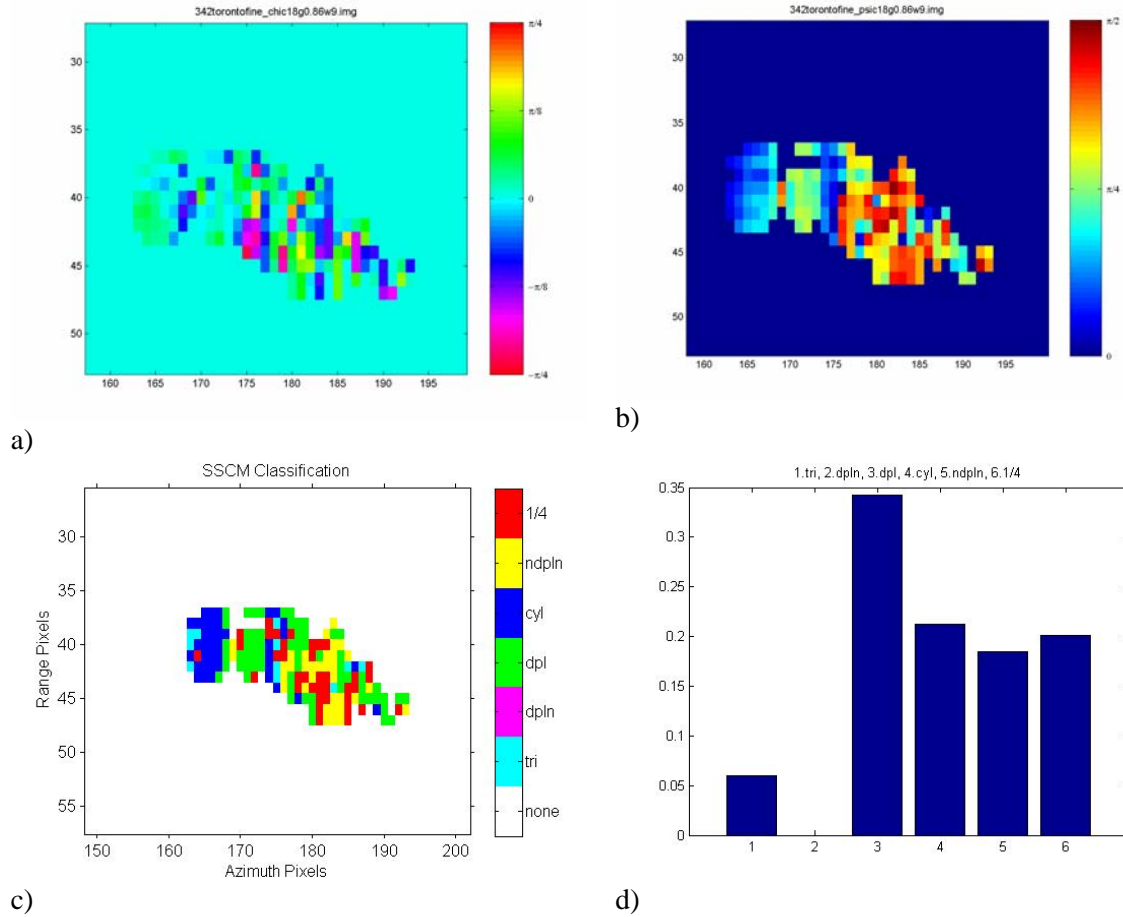


Figure 17: SSCM results of HMCS Toronto (l22p2, 17 October 2005) of Fine Quad-Pol Mode. a) latitude; b) longitude; c) classification and d) classification histogram.

In a) and b): azimuth pixels are along the x-axis and range pixels are along the y-axis. In d): the scatterer type is along the x-axis and the percentage of the distribution is along the y-axis.

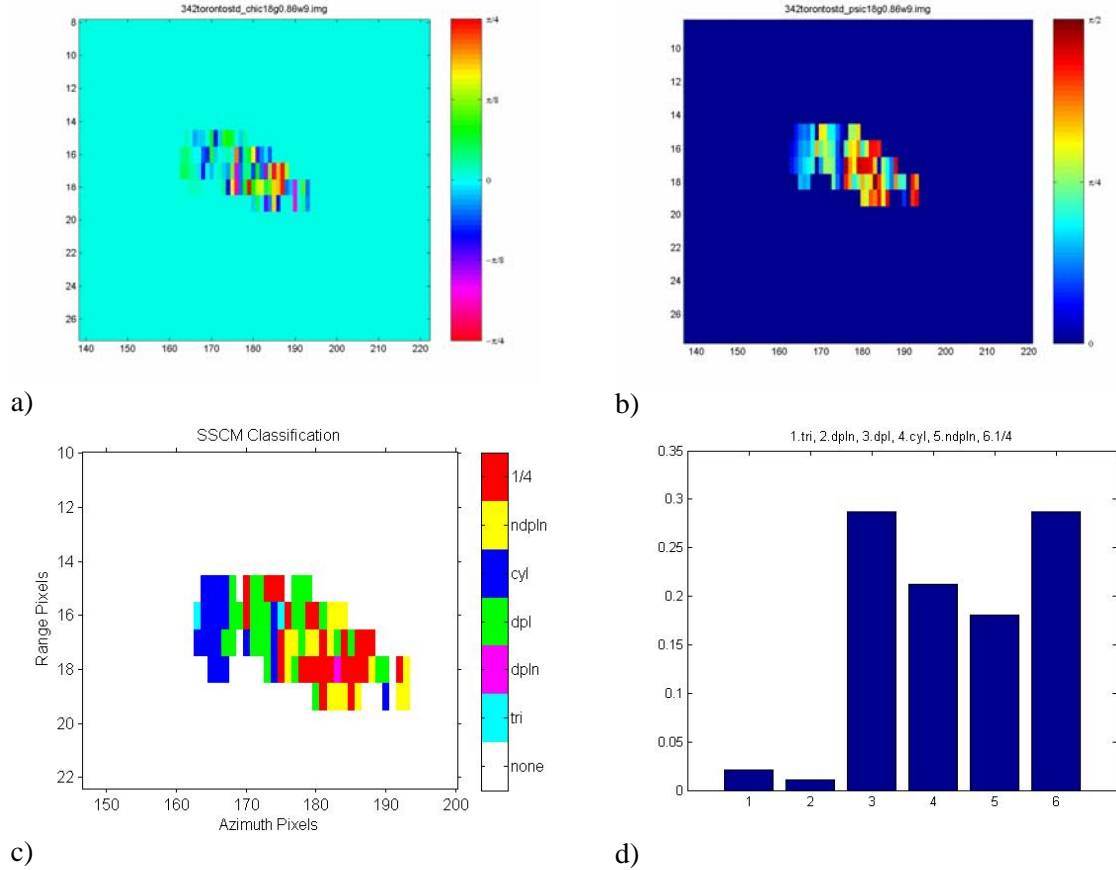


Figure 18: SSCM results of HMCS Toronto (l22p2, 17 October 2005) of Standard Quad-Pol Mode.
 a) latitude; b) longitude; c) classification and d) classification histogram.

In a) and b): azimuth pixels are along the x-axis and range pixels are along the y-axis. In d): the scatterer type is along the x-axis and the percentage of the distribution is along the y-axis.

Table 12: Summary of element scatterer distributions of SSCM decomposition for Fine Quad-Pol Mode.

Ship name	trihedral	diplane	dipole	cylinder	narrow diplane	quarter wave
17 Oct. 2005, l22p2 (a342)						
Gulf Service	0	0	0	0	1	0
HMCS Toronto	0.0598	0	0.03424	0.2120	0.1848	0.2011
20 Oct. 2005, Dominion Victory						
l41p1 (a358)	0	0	0.6667	0.2222	0	0.1111

Table 13: Summary of element scatterer distributions of SSCM decomposition for Standard Quad-Pol Mode.

Ship name	trihedral	diplane	dipole	cylinder	narrow diplane	quarter wave
17 Oct. 2005, l22p2 (a342)						
<i>Gulf Service</i>	0	0	0	0	1	0
<i>HMSC Toronto</i>	0.0213	0.0106	0.2872	0.2128	0.1809	0.2872
20 Oct. 2005, Dominion Victory						
l41p1 (a358)	0	0	0.75	0.25	0	0

7 Summary and conclusions

The simulated RADARSAT-2 polarimetric products from the MARSIE trial data have been used to study the polarimetric signature of ships. The RADARSAT-2 simulator (RSAT2SIMU) simulates RADARSAT-2 products using EC CV-580 single-look complex data by increasing the noise floor and degrading the spatial resolution. However, the simulator can not simulate the geometry of RADARSAT-2, such as the altitude, incidence angle, and swath coverage. The simulated data quality depends on the input CV-580 data quality.

The results demonstrate that polarimetric ship detection algorithms [4] and the classification methods, such as target decomposition ([5], [6], [7]), developed using airborne PolSAR data will potentially be applicable to RADARSAT-2 products.

A total of 5 simulated images of various ships have been studied to date; it is clear that polarimetric SAR can be used to improve ship detection and to provide the surveillance operator with some additional classification information. Polarimetric SAR provides both phase and amplitude information, which can reduce the false alarm rate and permit the detection of smaller ships than possible with single- or dual-channel SAR systems. For example, the ship, *Dominion Victory*, having a length of 25 m, was not detected using either single channel in most cases, or by a dual-channel system in some cases.

For the ship detection, the results clearly show the advantage of polarimetry. Small ships often cannot be detected using single channel systems. The dual co-polarization system with phase provides better detection performance than single channel HH polarization. However, dual co-polarization system should provide wider coverage than polarimetric systems.

Three polarimetric target decomposition methods were applied to characterize the targets of interest in terms of their elemental scatterers. These methods included Pauli, Cameron, and SSCM. Each method provided different information about the target. The Cameron and SSCM target decomposition methods provide unique information on the distribution and types of scatterers that constitute the target of interest, providing an approach for target classification. These decomposition methods work best for well-focused, large ships. The Pauli decomposition method provides a simple but efficient way to distinguish the target of interest (predominantly double bounce scattering) from the surrounding ocean (predominantly single bounce scattering).

Decomposition results from the considered methods should be combined with other target metrices such as signature length, signature cross section, and derived tar motion to aid in target classification.

Based upon our analysis, the following issues are recommended for further study:

- The relationship between target features and the elemental scatterers derived from the Cameron and the SSCM polarimetric decomposition methods;
- The relationship between target features and the polarimetric signature; and

- The feasibility of applying polarimetric target analysis methods to automatic target recognition by using scattering elements as target features in target classification software such as the ATR Workbench [15].

References

- [1] (Online); <http://www.radarsat2.info/>; Jan. 11, 2007.
- [2] MDA; RADARSAT-2 Polarimetric Product Simulation Tool (RSAT2SIMU); March 2004.
- [3] Vachon, W.P, M. Dragošević, N. Kashyap, C. Liu, D. Schlingmeier, A. Meek, T. Potter, B. Yue and J. Kraft; Processing and Analysis of Polarimetric Ship Signatures from MARSIE – Report on Results for Polar Epsilon; DRDC Ottawa TM 2006-202, Defence R&D Canada – Ottawa, 2006.
- [4] Liu, C., P.W. Vachon and G.W. Geling; Improved ship detection using polarimetric SAR data; *Canadian Journal of Remote Sensing*, Vol. 31, No. 1, pp 122-131, 2005.
- [5] Cloude, S.R., and E. Pottier; A Review of Target Decomposition Theorems in Radar Polarimetry; *IEEE Transactions on Geoscience and Remote Sensing*, Vol. 34, No. 2, pp 498-518, 1996.
- [6] Cameron, W.L., N.N. Youssef, and L.K. Leung; Simulated Polarimetric Signatures of Primitive Geometrical Shapes; *IEEE Transactions on Geoscience and Remote Sensing*, Vol. 34, No. 3, pp 793-803, 1996.
- [7] Touzi, R., F. Charbonneau, R.K. Hawkins, and P.W. Vachon; Ship detection and characterization using polarimetric SAR; *Canadian Journal of Remote Sensing*, Vol. 30, No. 3, pp 552-559, 2004.
- [8] Ulaby, F.T. and C. Elachi (Editors); Radar Polarimetry for Geoscience Applications; Artech House, Inc. 1990.
- [9] Touzi, R. and F. Charbonneau; User Guide Polarimetric Workstation; Canada Center for Remote Sensing Natural Resources Canada, March 2004.
- [10] Vachon, P.W. and M.V. Dragošević; The COASP and CHASP processors for strip-map and moving target adaptive processing of EC CV-580 synthetic aperture radar data; DRDC Ottawa TM 2006-006, Defence R&D Canada – Ottawa, 2006.
- [11] Scharf, L.L.; Statistical Signal Processing – Detection, Estimation, and Time Series Analysis; Addison-Wesley Publishing Company, 1991.
- [12] Liu, C. and G.H. Gierull; Using ambiguities to aid in moving target detection in PolSAR images; *EUSAR 2006 conference proceedings*, Dresden, Germany, 16-18 May, 2006.
- [13] Pottier, E.; Polarimetry: From Basics to Applications; *IGARSS 2003*, Toulouse, France, 21-25 July 2003.
- [14] Yeremy, M., J.W.M. Campbell, K. Mattar, and T. Potter; Ocean Surveillance with Polarimetric SAR; *Canadian Journal of Remote Sensing*, Vol. 27, No. 4, 2001, pp 328-343.
- [15] Norris, J., P.W. Vachon, D. Schlingmeier, R. English and L. Gallop; Expendable Trihedral Corner Reflectors for Target Enhancement and Position Control in RADARSAT-1 Fine Beam Mode SAR Imagery: Results from an Exercise Narwhal Pre-Trial Deployment; DRDC Ottawa TM 2004-197, Defence R&D Canada – Ottawa, 2006.

- [16] English, R.A., S.J. Rawlinson, and N.M. Sandirasegaram; ATR Workbench for Automating Image Analysis; Algorithms for Synthetic Aperture Radar Imagery X, Proceedings of SPIE Vol. 5095, pp 349-357, 2003.
- [17] Livingstone, C.E., A.L. Gray, R.K. Hawkins, P.W. Vachon, T.I. Lukowski and M. Lalonde; The CCRS Airborne SAR Systems: Radar for Remote Sensing Research; *Canadian Journal of Remote Sensing*, Vol. 21, p. 468-491, 1995.

Annex A Simulated RADARSAT-2 images

The simulated RADARSAT-2 images of *Dominion Victory* from four flight passes on 20 October 2005 and one flight pass which contains three known vessels on 17 October 2005 are presented in this Annex. The *Dominion Victory* from l41p2 and *Edward CornWallis* from l22p2 are not visible in the simulated images.

In the figures in this Annex, azimuth pixels are along the x-axis and range pixels are along the y-axis.

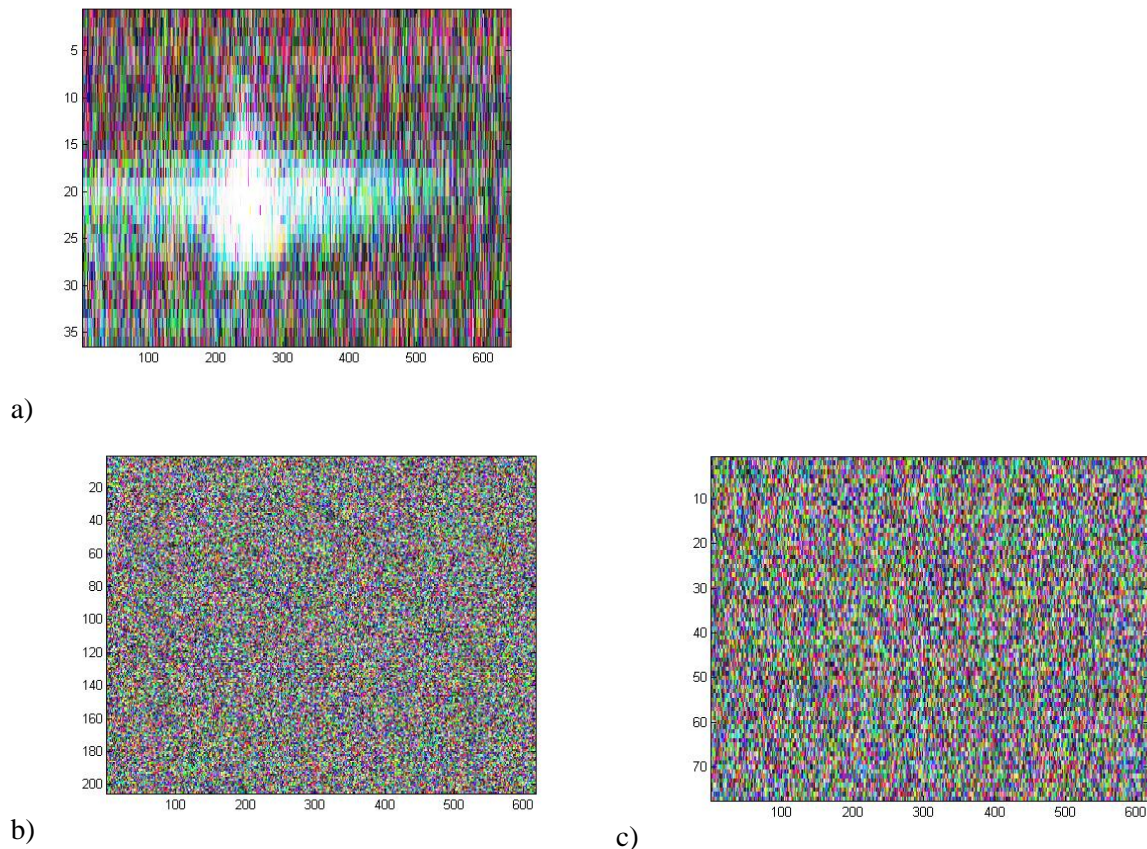
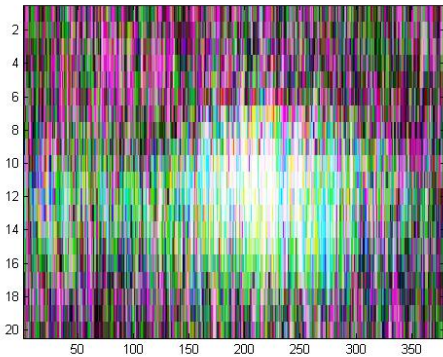
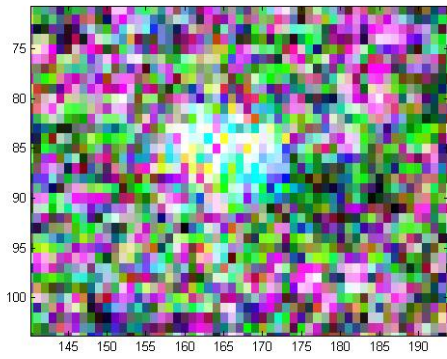


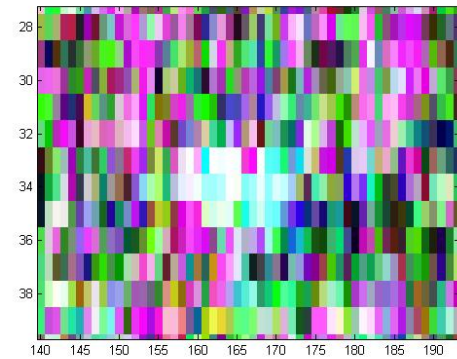
Figure 19: Polarimetric image of *Dominion Victory* (l41p2, 20 October 2005). a) CV-580 image; b) Fine Quad-Pol Mode; c) Standard Quad-Pol Mode.



a)



b)



c)

Figure 20: Polarimetric image of Dominion Victory (l41p3, 20 October 2005). a) CV-580 image; b) Fine Quad-Pol Mode; c) Standard Quad-Pol Mode.

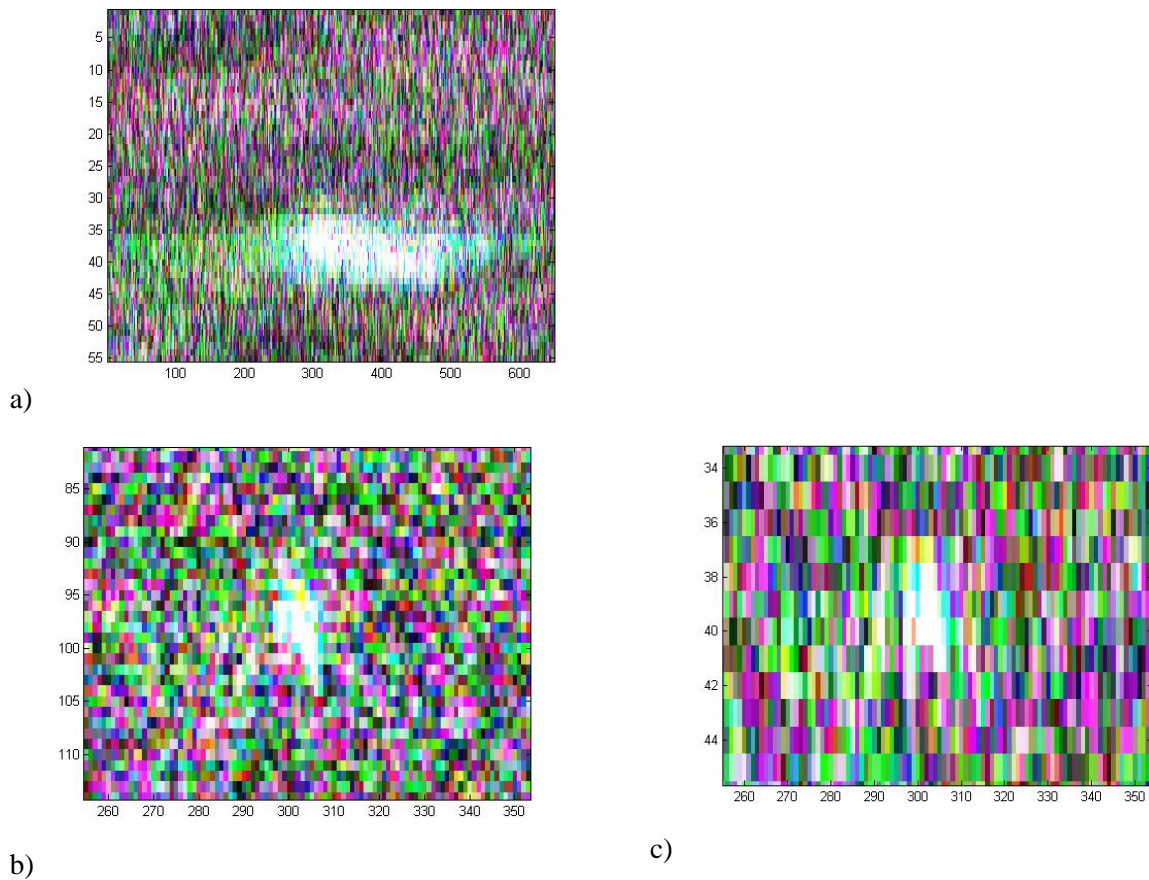
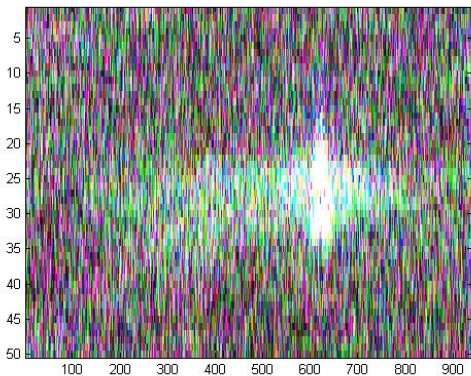
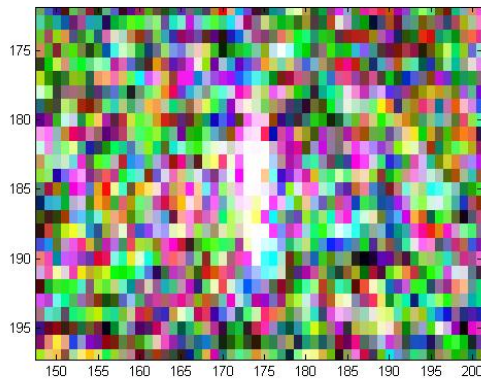


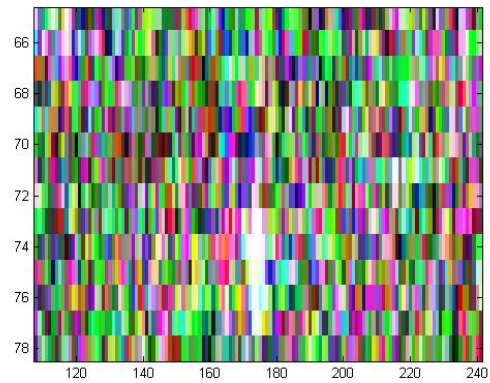
Figure 21: Polarimetric image of Dominion Victory (l42p4, 20 October 2005). a) CV-580 image; b) Fine Quad-Pol Mode; c) Standard Quad-Pol Mode.



a)

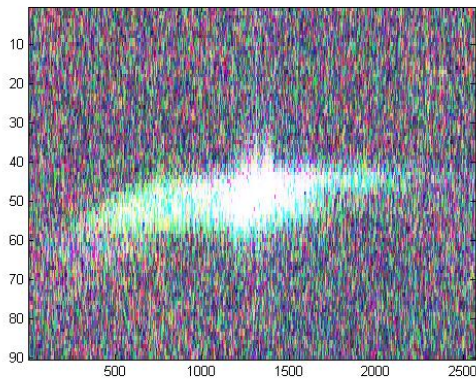


b)

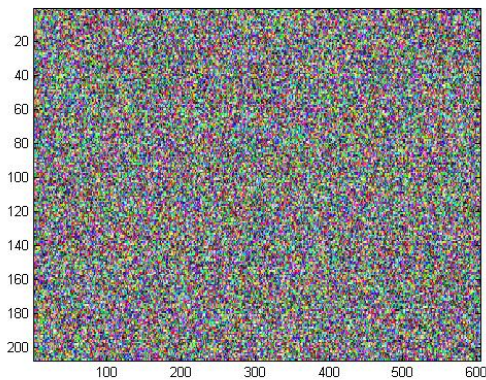


c)

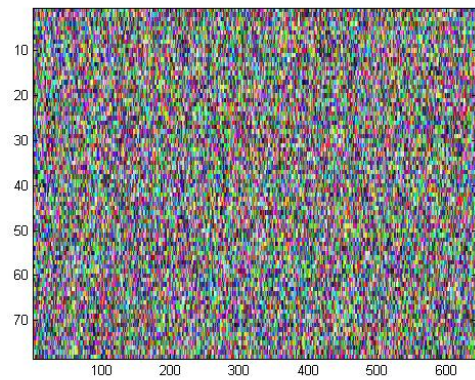
Figure 22: Polarimetric image of Gulf Service (l22p2, 17 October 2005). a) CV-580 image; b) Fine Quad-Pol Mode; c) Standard Quad-Pol Mode.



a)

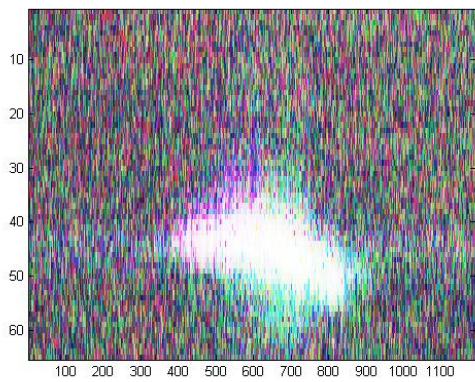


b)

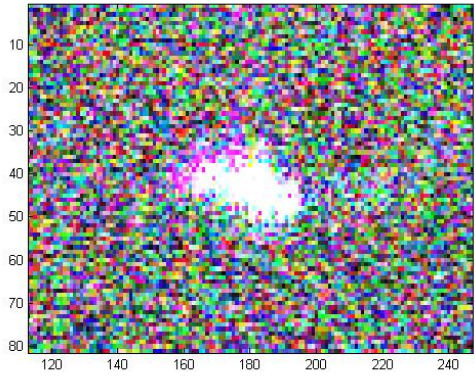


c)

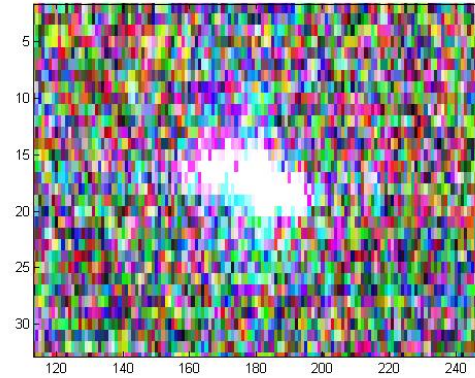
Figure 23: Polarimetric image of Edward Cornwallis (l22p2, 17 October 2005). a) CV-580 image; b) Fine Quad-Pol Mode; c) Standard Quad-Pol Mode.



a)



b)

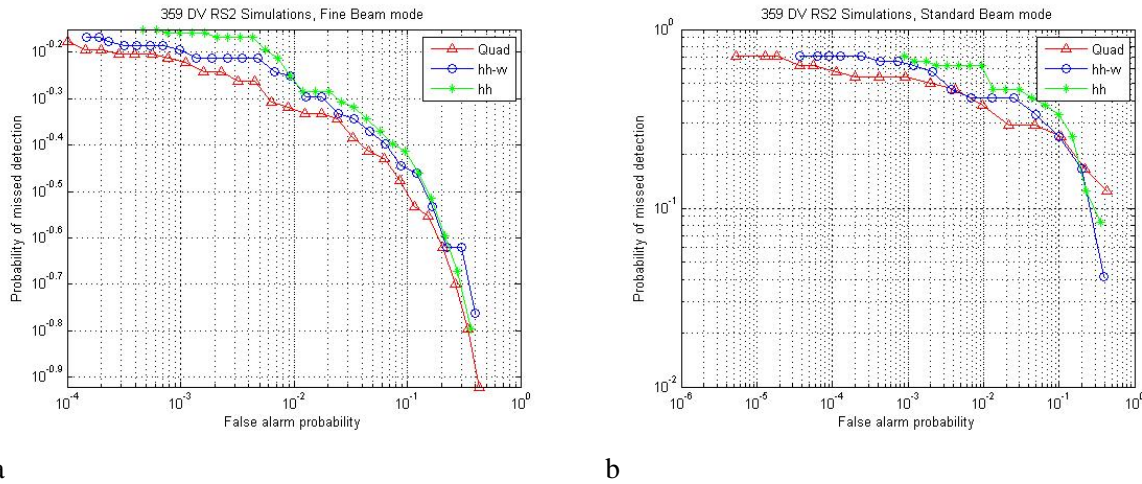


c)

Figure 24: Polarimetric image of HMCS Toronto (l22p2, 17 October 2005). a) CV-580 image; b) Fine Quad-Pol Mode; c) Standard Quad-Pol Mode.

Annex B ROC

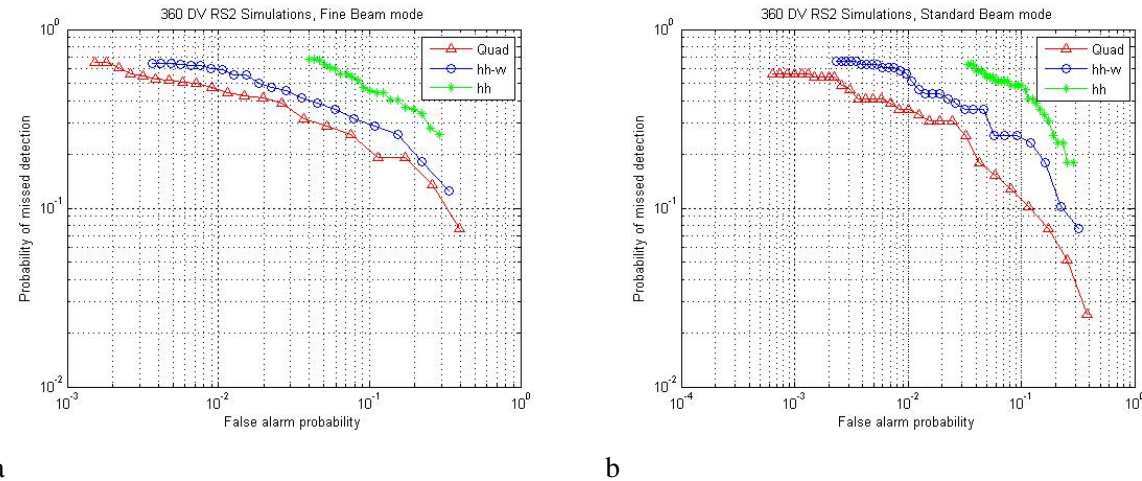
The ROC results of cases studied are presented in this Annex.



a

b

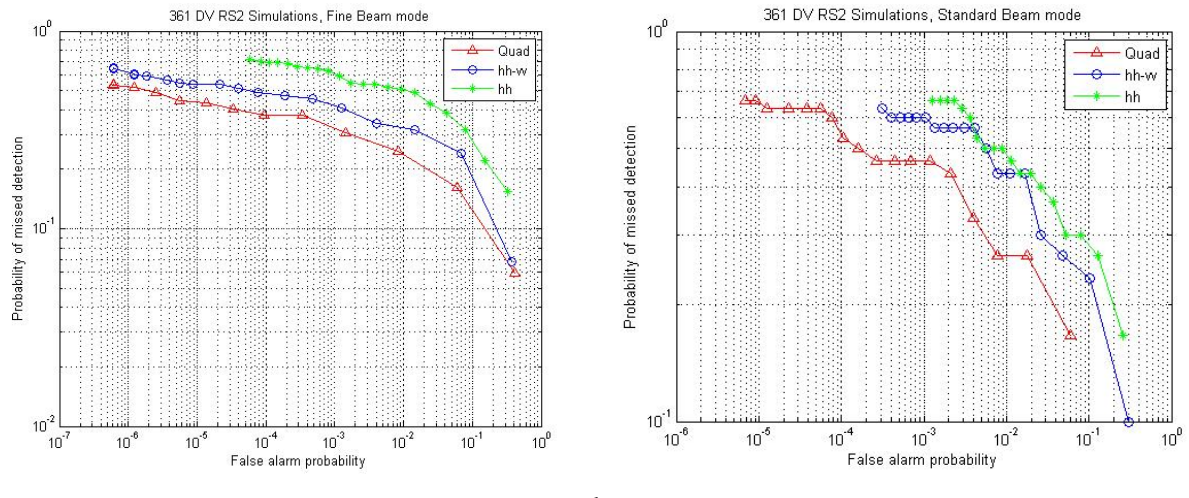
Figure 25: Detection performance for Dominion Victory (l41p2, 20 October 2005). a) Fine Quad-Pol Mode; b). Standard Quad-Pol Mode.



a

b

Figure 26: Detection performance for Dominion Victory (l41p3, 20 October 2005). a). Fine Quad-Pol Mode; b). Standard Quad-Pol Mode.



a

b

Figure 27: Detection performance for Dominion Victory (l42p4, 20 October 2005). a) Fine Quad-Pol Mode; b) Standard Quad-Pol Mode.

Annex C Pauli Decomposition Results

The Pauli decomposition results for the cases studied are presented in this Annex.

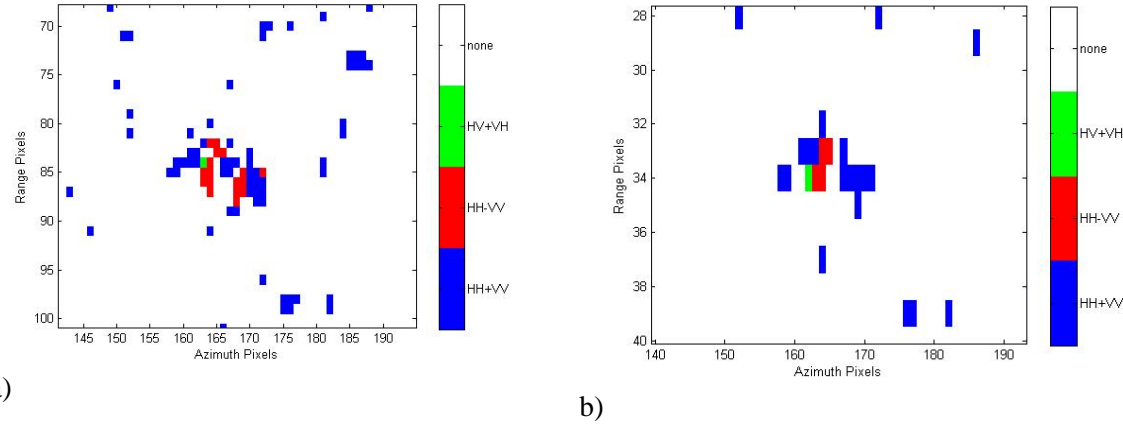


Figure 28: Pauli decomposition image of Dominion Victory (l41p3, 20 October 2005). a) Fine Quad-Pol Mode; b) Standard Quad-Pol Mode.

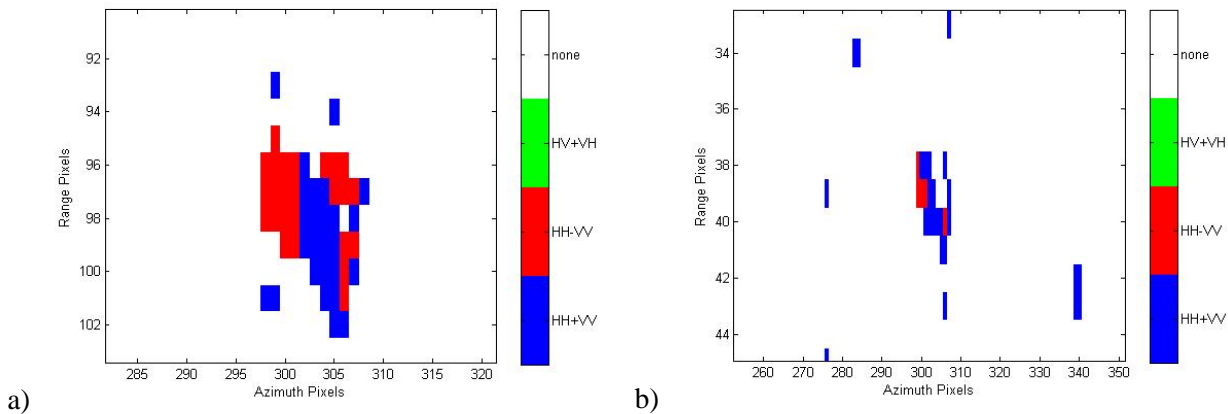


Figure 29: Pauli decomposition image of Dominion Victory (l42p2, 20 October 2005). a) Fine Quad-Pol Mode; b) Standard Quad-Pol Mode.

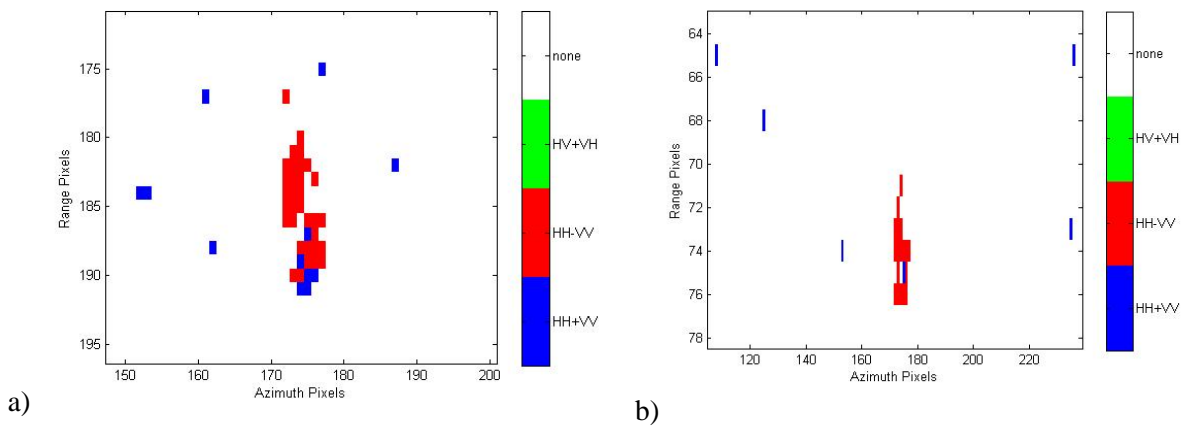


Figure 30: Pauli decomposition image of Gulf Service (l42p2, 17 October 2005). a) Fine Quad-Pol Mode; b) Standard Quad-Pol Mode.

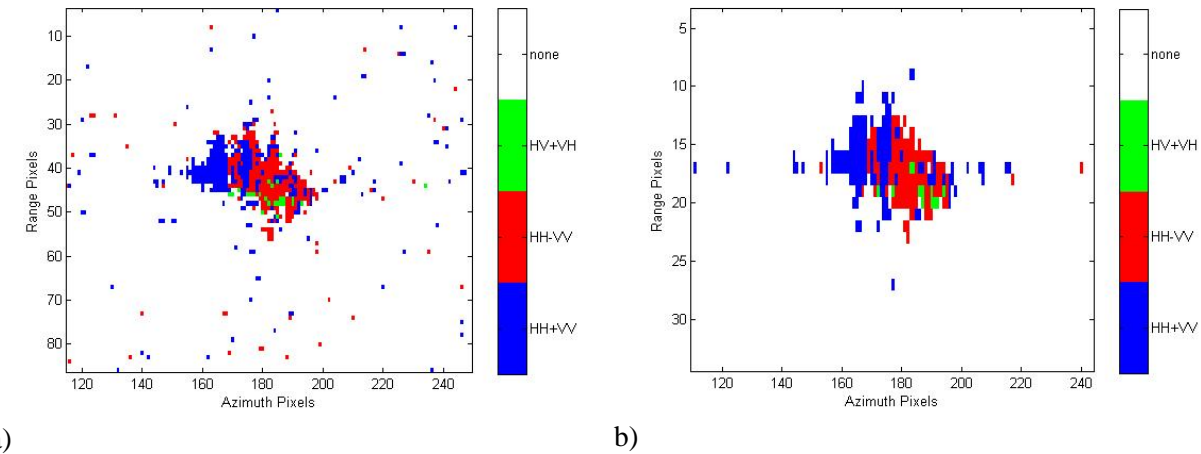


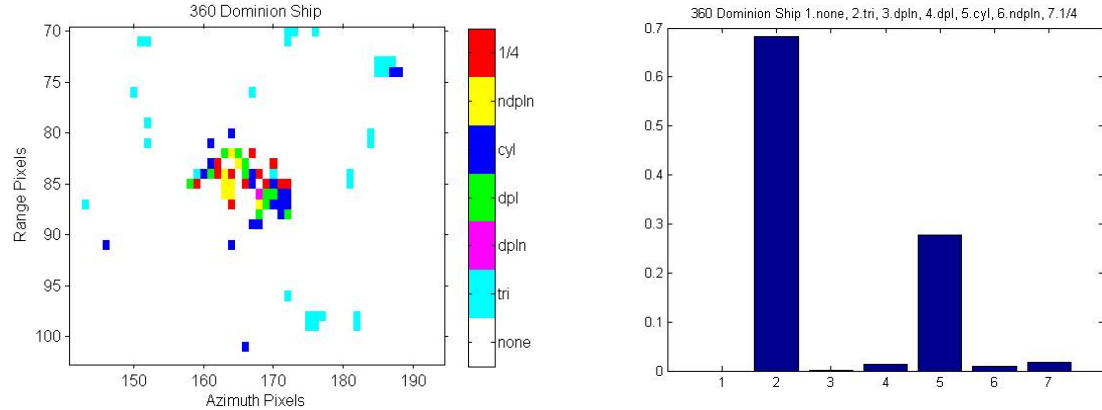
Figure 31: Pauli decomposition image of HMCS Toronto (l22p2, 17 October 2005). a) Fine Quad-Pol Mode; b) standard quad-plo Mode.

Annex D Cameron decomposition results

The Cameron decomposition results of cases studied are presented in this Annex.

In the histogram figures in this Annex: the scatterer type is along the x-axis and the percentage of the distribution is along the y-axis.

a)



b)

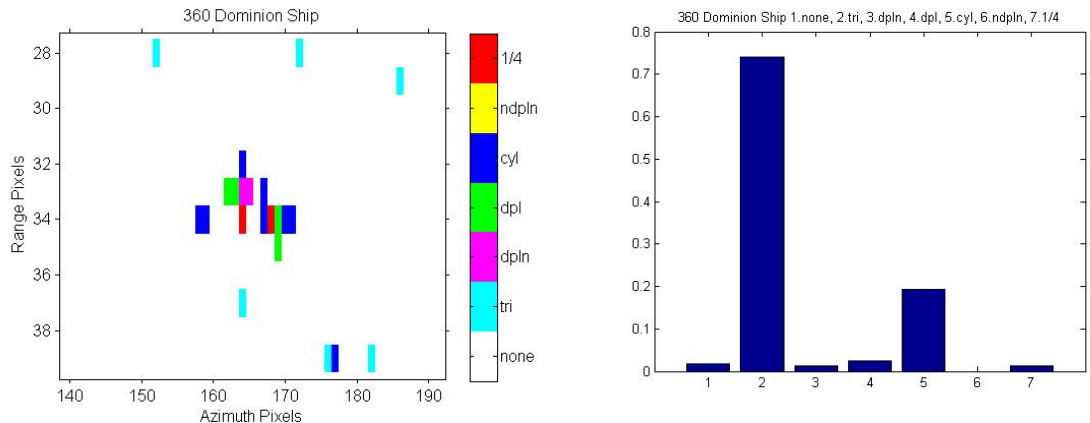
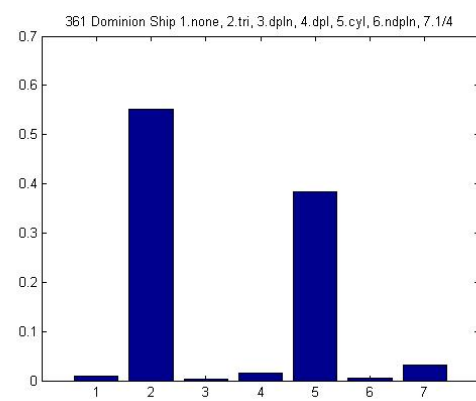
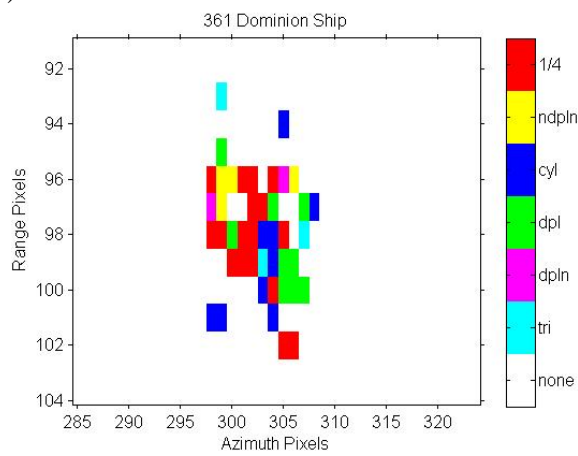


Figure 32: Cameron decomposition image and histogram of Dominion Victory (I41p3, 20 October 2005). a) Fine Quad-Pol Mode; b) Standard Quad-Pol Mode.

a)



b)

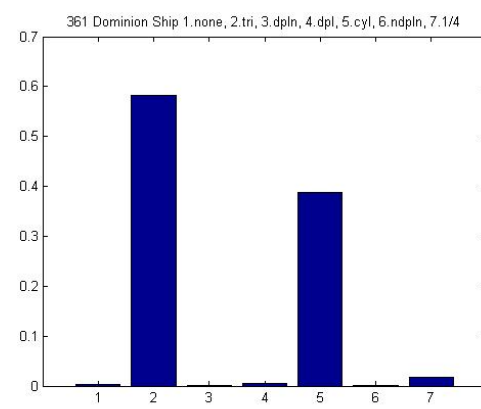
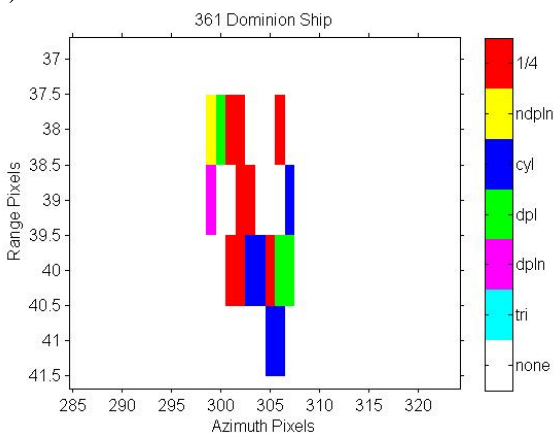
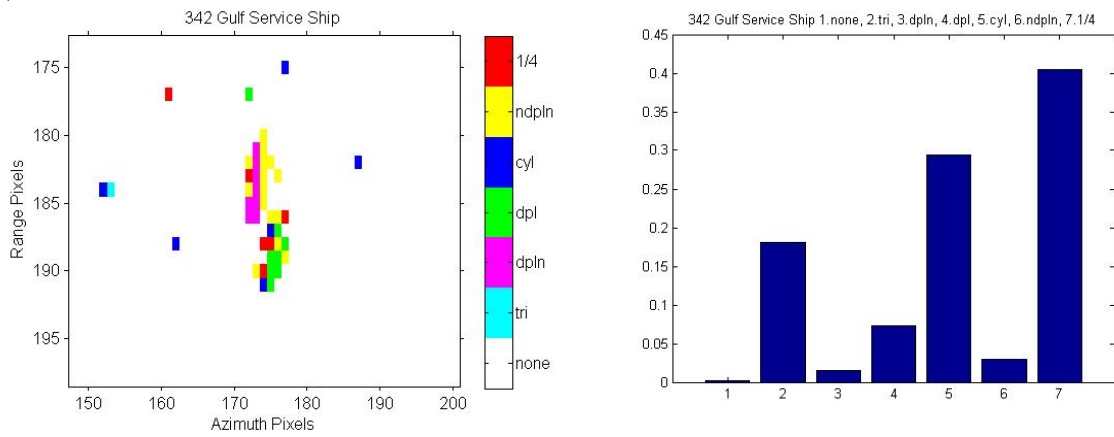


Figure 33: Cameran decomposition image and histogram of Dominion Victory (142p4, 20 October 2005). a) Fine Quad-Pol Mode; b) Standard Quad-Pol Mode.

a)



b)

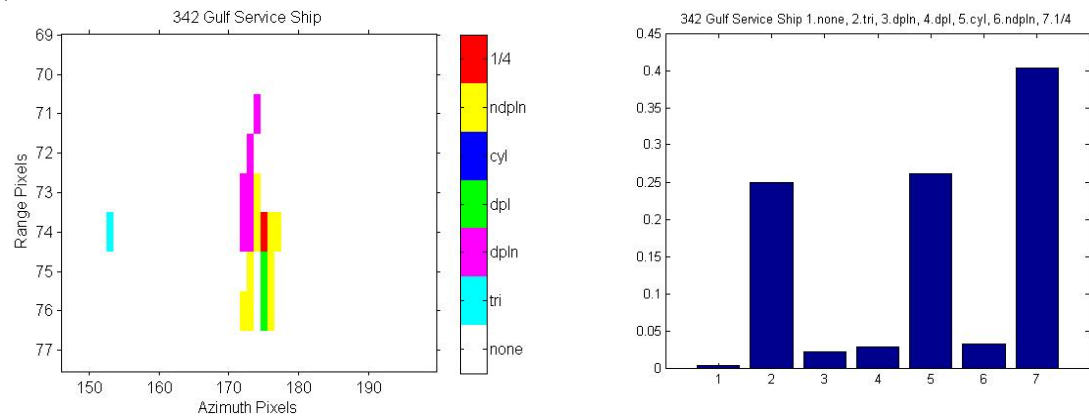
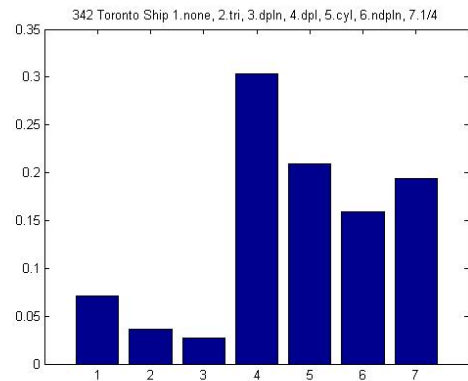
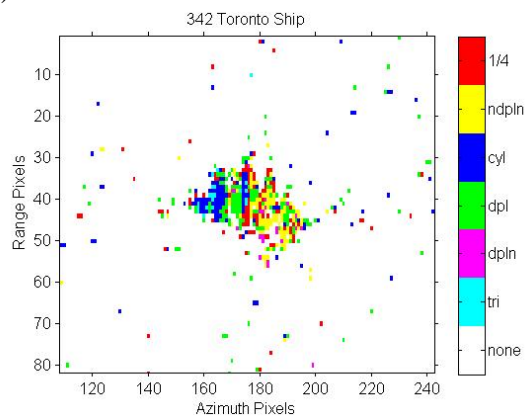


Figure 34: Cameron decomposition image and histogram of Gulf Service (l22p2, 17 October 2005). a) Fine Quad-Pol Mode; b) standard quad-plo Mode.

a)



b)

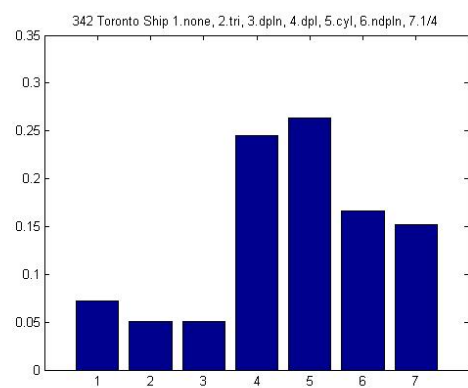
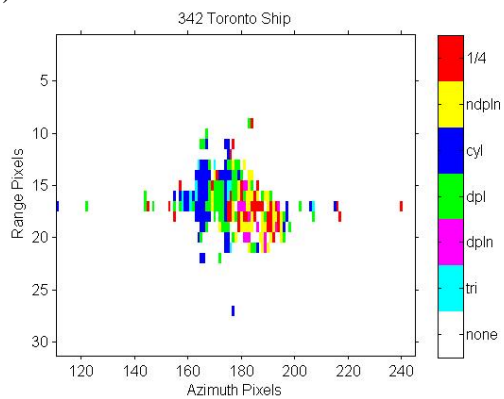


Figure 35: Cameron decomposition image and histogram of HMCS Toronto (l22p2, 17 October 2005). a) Fine Quad-Pol Mode; b) standard quad-plo Mode.

Annex E SSCM decomposition results

The results of the SSCM decomposition are presented in this Annex. There weren't any coherent targets detected in 141p3 or 142p4.

In the figures in this Annex, a) and b): azimuth pixels are along the x-axis and range pixels are along the y-axis; d): the scatterer type is along the x-axis and the percentage of the distribution is along the y-axis.

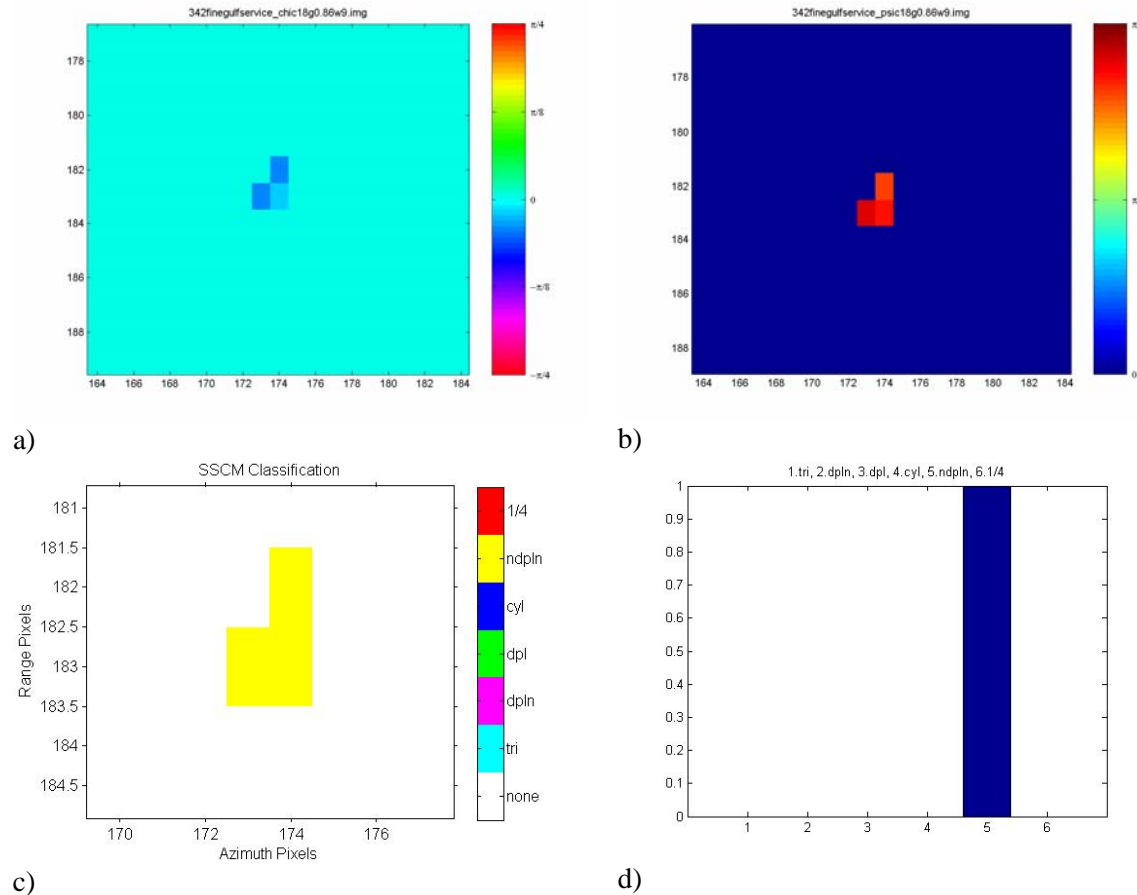


Figure 36: SSCM decomposition images Gulf Service for Fine Quad-Pol Mode (l22p2, 17 October 2005). a) latitude; b) longitude; c) classification; d) histogram.

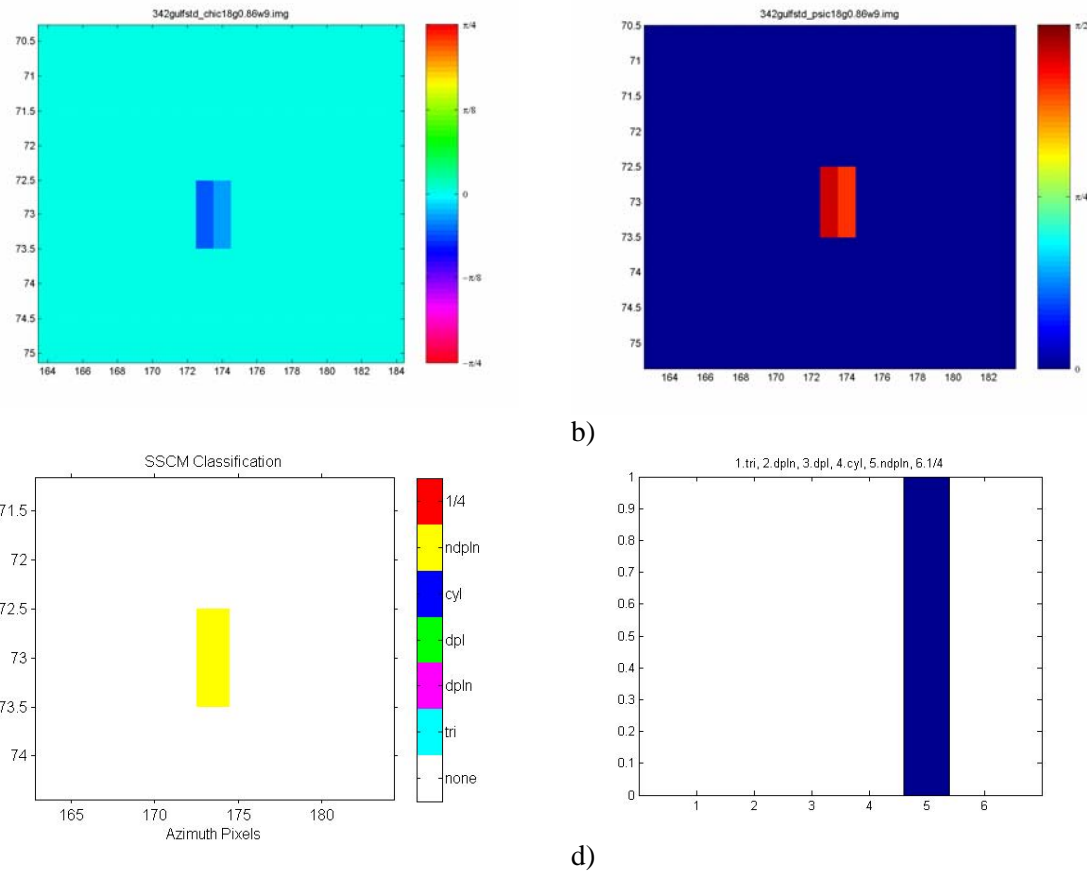


Figure 37: SSCM decomposition images of Gulf Service for Standare Quad-Pol Mode (l22p2, 17 October 2005). a) latitude; b) longitude; c) classification; d) histogram.

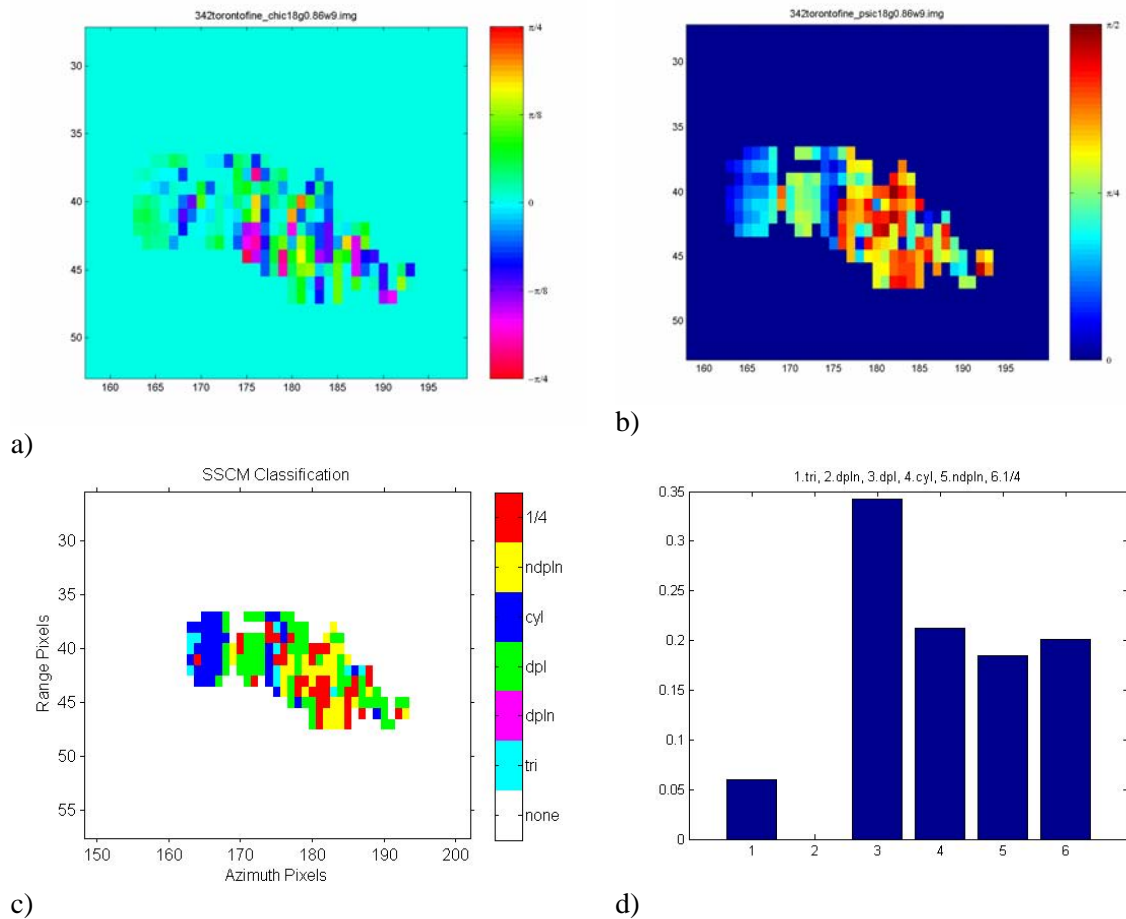


Figure 38: SSCM decomposition images of Toronto for Fine Quad-Pol mode (l22p2, 17 October 2005). a) latitude; b) longitude; c) classification; d) histogram.

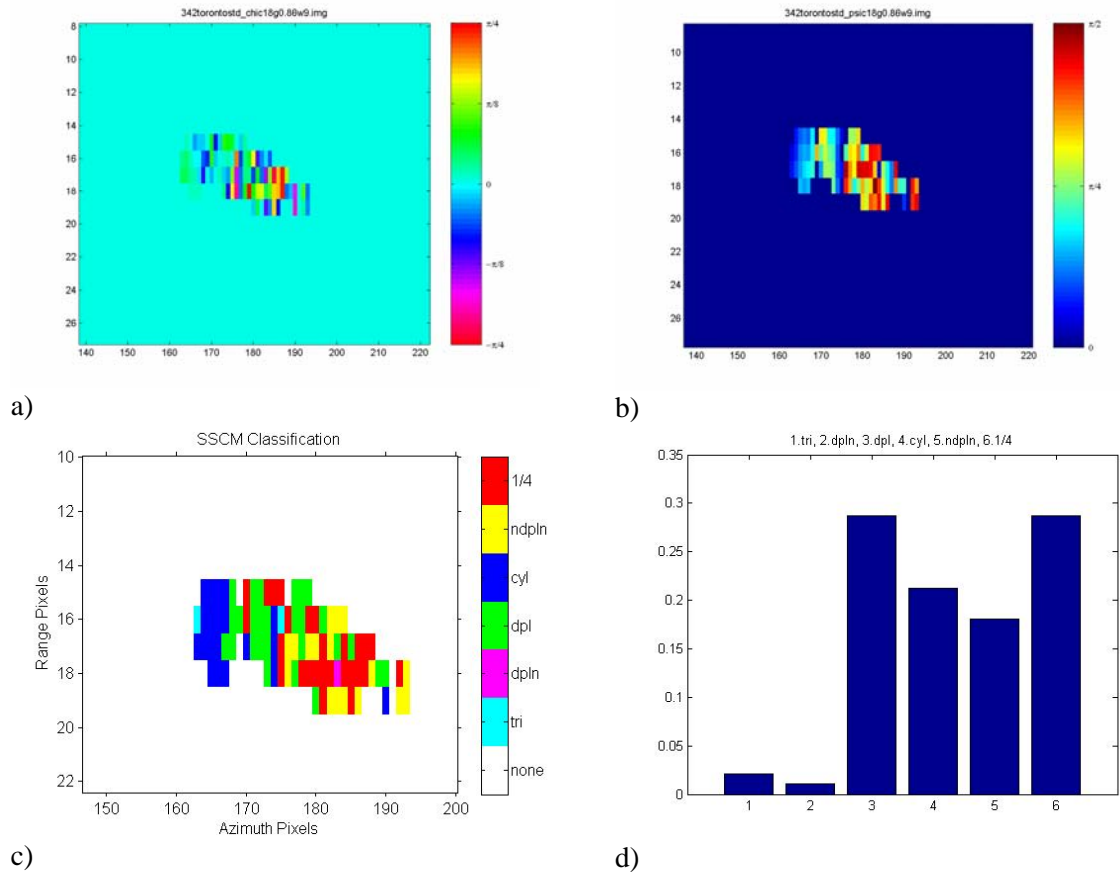


Figure 39: SSCM decomposition images of Toronto for Standard Quad-Pol mode ($l22p2$, 17 October 2005). a) latitude; b) longitude; c) classification; d) histogram.

Annex F Ship photos

The photographs of the ships studied are shown in this Annex. These photos were taken during the MARSIE trial by Janice Lang (DRDC Ottawa).



a)



b)



c)

Figure 40: Ship photographs: a) Dominion Victory; b) HMCS Toronto; c) Gulf Service.

List of symbols/abbreviations/acronyms/initialisms

CCRS	Canada Center for Remote Sensing
CSA	Canadian Space Agency
CHASP	Chip-Based Adaptive SAR Processor
COASP	Configurable Airborne SAR Processor
DRDC	Defence R&D Canada
EC	Environment Canada
Geotiff	Geographic Tagged Image File Format
HH	Horizontal-Horizontal
HV	Horizontal-Vertical
LUT	Look-Up Table
MARSIE	Maritime Sensor Integration Experiment
NESZ	Noise Equivalent Signal Zero
P_{FA}	Probability of False Alarm
P_{MD}	Probability of Missed Detection
PCR	Peak-to-Clutter Ratio
PolInSAR	Polarimetric SAR Interferometry
PolSAR	Polarimetric Synthetic Aperture Radar
ROC	Receiver Operating Characteristic
SAR	Synthetic Aperture Radar
SLC	Single Look Complex
SSCM	Symmetric Scattering Characterization Method
TTCP	The Technical Cooperation Program
VH	Vertical-Horizontal
VV	Vertical-Vertical
XML	eXtensible Markup Language

Distribution list

Document No.: DRDC Ottawa TM 2007-189

LIST PART 1: Internal Distribution by Centre:

4 Library DRDC Ottawa
1 English, Ryan
1 Geling, Gary
2 Liu, Chen
1 Livingstone, Chuck
1 Sabry, Ramin
1 Schlingmeier, David
1 Secker, Jeff
1 Vachon, Paris

13 TOTAL LIST PART 1

LIST PART 2: External Distribution by DRDKIM

1 DRDKIM
2 Library and Archives Canada
1 CISTI
1 Butler, Maj Peter, DJCP
1 Howes, LCol Jeff, DPDOIS, Polar Epsilon
1 Quinn, LCdr Robert, DJCP
1 Samoluk, LCdr Andy, DJCP
1 Tunaley, J.K.E., DPDOIS, Polar Epsilon
1 Wilcox, Caroline, DSTC4ISR

10 TOTAL LIST PART 2

23 TOTAL COPIES REQUIRED

This page is intentionally left blank

DOCUMENT CONTROL DATA

(Security classification of title, body of abstract and indexing annotation must be entered when the overall document is classified)

<p>1. ORIGINATOR (The name and address of the organization preparing the document. Organizations for whom the document was prepared, e.g. Centre sponsoring a contractor's report, or tasking agency, are entered in section 8.)</p> <p>Defence R&D Canada - Ottawa 3701 Carling Avenue Ottawa, Ontario, K1A 0Z4 Canada</p>		<p>2. SECURITY CLASSIFICATION (Overall security classification of the document including special warning terms if applicable.)</p> <p>UNCLASSIFIED</p>	
<p>3. TITLE (The complete document title as indicated on the title page. Its classification should be indicated by the appropriate abbreviation (S, C, R or U) in parentheses after the title.)</p> <p>Evaluation of Simulated RADARSAT-2 Polarimetry Products</p>			
<p>4. AUTHORS (last name, followed by initials – ranks, titles, etc. not to be used)</p> <p>Liu, Chen; Vachon, Paris W.</p>			
<p>5. DATE OF PUBLICATION (Month and year of publication of document.)</p> <p>September 2007</p>		<p>6a. NO. OF PAGES (Total containing information, including Annexes, Appendices, etc.)</p> <p>73</p>	<p>6b. NO. OF REFS (Total cited in document.)</p> <p>16</p>
<p>7. DESCRIPTIVE NOTES (The category of the document, e.g. technical report, technical note or memorandum. If appropriate, enter the type of report, e.g. interim, progress, summary, annual or final. Give the inclusive dates when a specific reporting period is covered.)</p> <p>Technical Memorandum</p>			
<p>8. SPONSORING ACTIVITY (The name of the department project office or laboratory sponsoring the research and development – include address.)</p> <p>DRDC Ottawa</p>			
<p>9a. PROJECT OR GRANT NO. (If appropriate, the applicable research and development project or grant number under which the document was written. Please specify whether project or grant.)</p> <p>15ec05</p>		<p>9b. CONTRACT NO. (If appropriate, the applicable number under which the document was written.)</p>	
<p>10a. ORIGINATOR'S DOCUMENT NUMBER (The official document number by which the document is identified by the originating activity. This number must be unique to this document.)</p> <p>DRDC Ottawa TM 2007-189</p>		<p>10b. OTHER DOCUMENT NO(s). (Any other numbers which may be assigned this document either by the originator or by the sponsor.)</p>	
<p>11. DOCUMENT AVAILABILITY (Any limitations on further dissemination of the document, other than those imposed by security classification.)</p> <p>(X) Unlimited distribution <input type="checkbox"/> Defence departments and defence contractors; further distribution only as approved <input type="checkbox"/> Defence departments and Canadian defence contractors; further distribution only as approved <input type="checkbox"/> Government departments and agencies; further distribution only as approved <input type="checkbox"/> Defence departments; further distribution only as approved <input type="checkbox"/> Other (please specify):</p>			
<p>12. DOCUMENT ANNOUNCEMENT (Any limitation to the bibliographic announcement of this document. This will normally correspond to the Document Availability (11). However, where further distribution (beyond the audience specified in (11) is possible, a wider announcement audience may be selected.)</p>			

13. **ABSTRACT** (A brief and factual summary of the document. It may also appear elsewhere in the body of the document itself. It is highly desirable that the abstract of classified documents be unclassified. Each paragraph of the abstract shall begin with an indication of the security classification of the information in the paragraph (unless the document itself is unclassified) represented as (S), (C), (R), or (U). It is not necessary to include here abstracts in both official languages unless the text is bilingual.)

This report presents an evaluation of simulated RADARSAT-2 polarimetry products. The RSAT2SIMU software developed by MDA simulates RADARSAT-2 products from Environment Canada (EC) CV-580 synthetic aperture radar (SAR) single-look complex (SLC) data by increasing the noise floor and degrading the image resolution. The evaluation includes observations of the reduction in the probability of missed detection for polarimetric relative to single channel radar operation for ship detection, and the potential benefit of polarimetric target decomposition to generate ship target classification features and to segment the ship target of interest from the ocean background. A main recommendation is to develop algorithms that combine all information available from polarimetric signature analysis methods to aid in ship classification. The results show that the ship detection and target classification methods developed using airborne polarimetric data can potentially be applied to RADARSAT-2 data.

14. **KEYWORDS, DESCRIPTORS or IDENTIFIERS** (Technically meaningful terms or short phrases that characterize a document and could be helpful in cataloguing the document. They should be selected so that no security classification is required. Identifiers, such as equipment model designation, trade name, military project code name, geographic location may also be included. If possible keywords should be selected from a published thesaurus, e.g. Thesaurus of Engineering and Scientific Terms (TEST) and that thesaurus identified. If it is not possible to select indexing terms which are Unclassified, the classification of each should be indicated as with the title.)

RADARSAT, SAR, synthetic aperture radar, polarimetry, polarization

Defence R&D Canada

Canada's leader in Defence
and National Security
Science and Technology

R & D pour la défense Canada

Chef de file au Canada en matière
de science et de technologie pour
la défense et la sécurité nationale



www.drdc-rddc.gc.ca